Cancer Cell

Article

Reduced Mitochondrial Apoptotic Priming Drives Resistance to BH3 Mimetics in Acute Myeloid Leukemia

Graphical Abstract

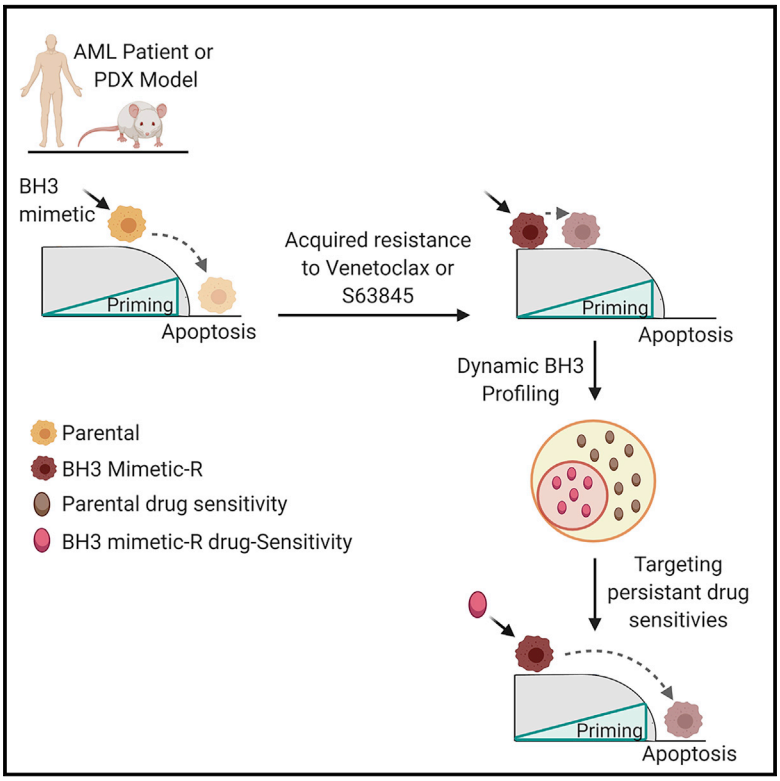

Highlights

- Reduced mitochondrial apoptotic priming drives acquired resistance to BH3 mimetics
- BH3 profiling predicts clinical response to venetoclax and HMA combinations
- Simultaneous BCL-2 and MCL-1 antagonism outperforms alternating regimens
- Dynamic BH3 profiling identifies drug vulnerabilities in BH3 mimetic-resistant AML

Authors

Shruti Bhatt, Marissa S. Pioso, Elyse Anne Olesinski, ..., David M. Weinstock, Jacqueline S. Garcia, Anthony Letai

Correspondence

anthony_letai@dfci.harvard.edu

In Brief

Bhatt et al. demonstrate that resistance to BCL-2 and MCL-1 antagonists emerges via selection for reduced mitochondrial apoptotic priming. Rapid measurements of drug-induced apoptotic signaling measured by dynamic BH3 profiling identify targeted agents with *in vivo* efficacy. BCL-2 and MCL-1 antagonist combinations overcome resistance to either single agent.

Bhatt et al., 2020, Cancer Cell *38*, 872–890
December 14, 2020
https://doi.org/10.1016/j.ccell.2020.10.010

CellPress

CellPress

Cancer Cell

Article

Reduced Mitochondrial Apoptotic Priming Drives Resistance to BH3 Mimetics in Acute Myeloid Leukemia

Shruti Bhatt,[1,2,3] Marissa S. Pioso,[1,2] Elyse Anne Olesinski,[1,2] Binyam Yilma,[1,2] Jeremy A. Ryan,[1,2] Thelma Mashaka,[1,2] Buon Leutz,[4] Sophia Adamia,[1] Haoling Zhu,[1] Yanan Kuang,[4] Abhishek Mogili,[4] Abner J. Louissaint,[1] Stephan R. Bohl,[1,2] Annette S. Kim,[2,6] Anita K. Mehta,[7] Sneha Sanghavi,[8] Youzhen Wang,[8] Erick Morris,[8] Ensar Halilovic,[8] Cloud P. Paweletz,[5] David M. Weinstock,[1,2] Jacqueline S. Garcia,[1] and Anthony Letai[1,2,9,10,*]

[1]Department of Medical Oncology, Dana-Farber Cancer Institute, 440 Brookline Avenue, M430, Boston, MA 02215, USA
[2]Harvard Medical School, Boston, MA, USA
[3]Department of Pharmacy, National University of Singapore, Singapore
[4]Department of Bioinformatics and Data Science, Dana-Farber Cancer Institute, Harvard Medical School, Boston, MA, USA
[5]Belfer Center for Applied Cancer Science, Dana-Farber Cancer Institute, Boston, MA, USA
[6]Brigham and Women's Hospital, Boston, MA, USA
[7]Breast Tumor Immunology Laboratory, Dana-Farber Cancer Institute, Boston, MA, USA
[8]Novartis Institutes for BioMedical Research, Inc., Cambridge, MA, USA
[9]Broad Institute of MIT and Harvard, Cambridge, MA, USA
[10]Lead Contact
*Correspondence: anthony_letai@dfci.harvard.edu
https://doi.org/10.1016/j.ccell.2020.10.010

SUMMARY

Acquired resistance to BH3 mimetic antagonists of BCL-2 and MCL-1 is an important clinical problem. Using acute myelogenous leukemia (AML) patient-derived xenograft (PDX) models of acquired resistance to BCL-2 (venetoclax) and MCL-1 (S63845) antagonists, we identify common principles of resistance and persistent vulnerabilities to overcome resistance. BH3 mimetic resistance is characterized by decreased mitochondrial apoptotic priming as measured by BH3 profiling, both in PDX models and human clinical samples, due to alterations in BCL-2 family proteins that vary among cases, but not to acquired mutations in leukemia genes. BCL-2 inhibition drives sequestered pro-apoptotic proteins to MCL-1 and vice versa, explaining why *in vivo* combinations of BCL-2 and MCL-1 antagonists are more effective when concurrent rather than sequential. Finally, drug-induced mitochondrial priming measured by dynamic BH3 profiling (DBP) identifies drugs that are persistently active in BH3 mimetic-resistant myeloblasts, including FLT-3 inhibitors and SMAC mimetics.

INTRODUCTION

The recent FDA approval of venetoclax in combination with hypomethylating agents (HMAs, including either azacitidine or decitabine) or low-dose cytarabine has expanded treatment options for newly diagnosed acute myelogenous leukemia (AML) patients medically unfit to receive induction therapy or aged 75 years or older (DiNardo et al., 2019; Konopleva and Letai, 2018; Wei et al., 2019, Wei et al., 2020). Venetoclax is a highly selective BCL-2 antagonist that eliminates BCL-2-dependent myeloblasts by displacing pro-apoptotic proteins from BCL-2, promoting oligomerization of BAX or BAK at the mitochondrial outer membrane (MOM) to initiate apoptosis (Souers et al., 2013; Pan et al., 2014; Vo et al., 2012). A 73% complete remission (CR) plus CR with incomplete count recovery rate was observed in treatment-naive AML patients treated with venetoclax plus an HMA, reaching a median overall survival of 17.3 months (DiNardo et al., 2019). Clinical predictive biomarkers are lacking and acquired resistance remains a clinical problem.

The clinical success of venetoclax in chronic lymphocytic leukemia (CLL) (Roberts et al., 2016) and AML (DiNardo et al., 2019; Wei et al., 2019) has spurred the development of an entire class of BH3 mimetic drugs that inhibit related anti-apoptotic proteins, including MCL-1 (e.g., S63845) (Caenepeel et al., 2018; Kotschy et al., 2016; Tron et al., 2018) and BCL-XL (Khan et al., 2019). The clinical derivative of S63845 (MIK665/S64315, co-developed by Servier and Novartis) is currently in phase I clinical development in AML/myelodysplastic syndrome (as monotherapy, NCT02979366, and combination with venetoclax, NCT: NCT03672695). Additional MCL-1 antagonists have since then followed, including VU661013 (Ramsey et al., 2018), AMG-176 (Caenepeel et al., 2018), and AZD-5991 (Tron et al., 2018), with the latter two under clinical investigation (NCT: NCT02675452 and NCT: NCT03218683) (Caenepeel et al., 2018; Tron et al., 2018; Ramsey et al., 2018). Although the

combination of BH3 mimetics (BCL-2 and MCL-1 antagonists) appears to be an attractive strategy to circumvent resistance based on preclinical studies, there are significant challenges, including toxicity concerns. MCL-1 antagonists bind human MCL-1 with stronger affinity than murine MCL-1 (Kotschy et al., 2016), thus limiting preclinical estimation of toxicity, including myocardial toxicity (Wang et al., 2013). Moreover, the kinetics of the combinatorial effect of BH3 mimetics on the sequestration of pro-apoptotic proteins by BCL-2 or MCL-1 has not been studied. Hence, guidance in scheduling these agents to achieve a maximal therapeutic index is limited.

Mechanisms underlying acquired resistance to BCL-2 antagonism in AML remain uncertain (Yecies et al., 2010). BCL-2 mutations Gly101Val, D103Y, Phe104Ile, and Gly33Arg have been described in CLL patients (Blombery et al., 2019; Tausch et al., 2019). Recently, four laboratories used loss-of-function CRISPR-Cas9 screens on venetoclax-resistant MOLM-13 or OCI-Ly1 cells to discover targetable liabilities in venetoclax-resistant setting. These studies revealed reliance of resistant cells on pro-survival BCL-2 family proteins, such as MCL-1, BCL-XL, and absence of pro-death proteins, TP53, NOXA, and BAX (Nechiporuk et al., 2019; Chen et al., 2019; Sharon et al., 2019; Guieze et al., 2019). They found targeting transmembrane receptors with tyrosine kinase (NTRK) (Nechiporuk et al., 2019), deletion of mitochondrial chaperon CLPB (Chen et al., 2019), inhibition of mitochondrial translation (Sharon et al., 2019), or combination with metabolic modulators (Guieze et al., 2019) as strategies to restore venetoclax sensitivity. Although these studies revealed potential therapeutic opportunities in the setting of venetoclax resistance, these findings were derived from cell line-based *in vitro* culture systems.

Due to the plurality of BCL-2 family proteins that collaborate to determine a response, protein and gene expression have been an inconsistent predictor of sensitivity to BH3 mimetics (Konopleva et al., 2016; Nangia et al., 2018; Konopleva and Letai, 2018). We have previously shown that directly probing cancer cell mitochondria with synthetic BH3 peptides that selectively interact with pro-survival BCL-2 family proteins can reveal dependence on BCL-2 or MCL-1 (Brunelle et al., 2009) by performing BH3 profiling. When the MOM permeabilization (MOMP) occurs robustly in response to BAD or MS-1 peptides, dependence on BCL-2 or MCL-1, respectively, can be inferred (Certo et al., 2006). Detection of BCL-2 dependence by BH3 profiling has accurately identified sensitivity to BCL-2 antagonism in many cell lines and primary human cancer systems, including AML (Vo et al., 2012), CLL (Del Gaizo Moore et al., 2007; Deng et al., 2007), ALL (Chonghaile et al., 2014; Del Gaizo Moore et al., 2008), and BPDCN (Montero et al., 2017).

Here, we aim to uncover determinants of resistance to BH3 mimetics in AML using patient samples and PDX models and to identify effective therapies to overcome resistance.

RESULTS

Baseline BH3 Profiling Predicts Response to Venetoclax and Hypomethylating Agents in AML

We previously observed that BH3 profiling of pretreatment myeloblasts predicts clinical response to single-agent venetoclax in the phase II trial of relapsed/refractory AML patients (Konopleva et al., 2016). Evaluating dependence on individual anti-apoptotic proteins relies on the selective binding pattern of BH3 peptides BAD, MS-1, and HRK to anti-apoptotic proteins (Figure 1A) (Certo et al., 2006). To ensure that our AML patient-derived xenograft (PDX) models bore similar determinants of venetoclax response to human clinical AML, we tested if BH3 profiling similarly predicted myeloblast sensitivity to venetoclax in both models. AML PDX-treated (Townsend et al., 2016) NSG mice received either 2 weeks of venetoclax or vehicle, and peripheral blasts were assessed on day 15 as a measure of *in vivo* efficacy (Figure 1B; Table S1). Consistent with previous findings in AML patients treated with venetoclax monotherapy (Konopleva et al., 2016), adding the mitochondrial priming response of the MS-1 peptide to that of HRK inversely correlated with the response to venetoclax in individual PDX models (Figures 1C and S1A). These results support the use of PDXs as relevant models of venetoclax sensitivity and resistance.

The addition of venetoclax to azacitidine greatly improved the response rate observed for either as a single agent in AML. We asked whether enhanced mitochondrial priming by azacitidine might provide a mechanistic explanation for this clinical synergy (DiNardo et al., 2019; Konopleva et al., 2016). We treated eight AML cell lines with azacitidine and performed dynamic BH3 profiling (DBP). DBP measures drug-induced apoptotic signaling, expressed as "delta priming," by comparing BH3 profiling of drug-treated and DMSO-treated cells (Montero et al., 2015). In the eight cell lines that we tested, azacitidine consistently enhanced overall mitochondrial priming (BIM peptide) and BCL-2 dependence (BAD peptide) (Figure 1D).

Since we found a mitochondrial basis for the clinical synergy of the combination of azacitidine and venetoclax, we next asked whether BH3 profiling (Figure 1E) predicted clinical response to the clinically relevant venetoclax + HMA combination as it did for single-agent venetoclax. The pretreatment bone marrow aspirates or peripheral blood (PB) from 19 patients (Table S2) were treated with venetoclax + HMA: 7 on clinical trial (NCT02203773) and 12 off-trial. The sum of response to both MS-1 and HRK peptides was again found to inversely relate to achievement of CR (Figure 1F) and performed well as a binary predictor of clinical response by receiver operating characteristic curve (Figure 1G). It was a better predictor than the BAD-HRK index of selective BCL-2 dependence in both the single agent and combination treatment contexts (Figure S1B). These results suggest that absence of resistance pathways (i.e., BCL-XL or MCL-1 dependence) is even more important than initial BCL-2 dependence when determining the best clinical response to venetoclax + HMA in AML at >30 days. Our results suggest that BH3 profiling similarly predicts human clinical and PDX responses to BH3 mimetics, supporting the utility of AML PDX models to study responses to venetoclax. We next asked if BH3 profiling can provide pharmacodynamic evidence for the MOM activity of venetoclax + HMA *in vivo*. BH3 profiling of patient myeloblasts during treatment revealed alterations in priming, consistent with an *in vivo* MOM mechanism of action (Figure S1C).

Modeling *In Vivo* Venetoclax Resistance in PDX Models of AML

Having observed a MOM mechanism underlying response to venetoclax, we wondered if mechanisms of resistance also

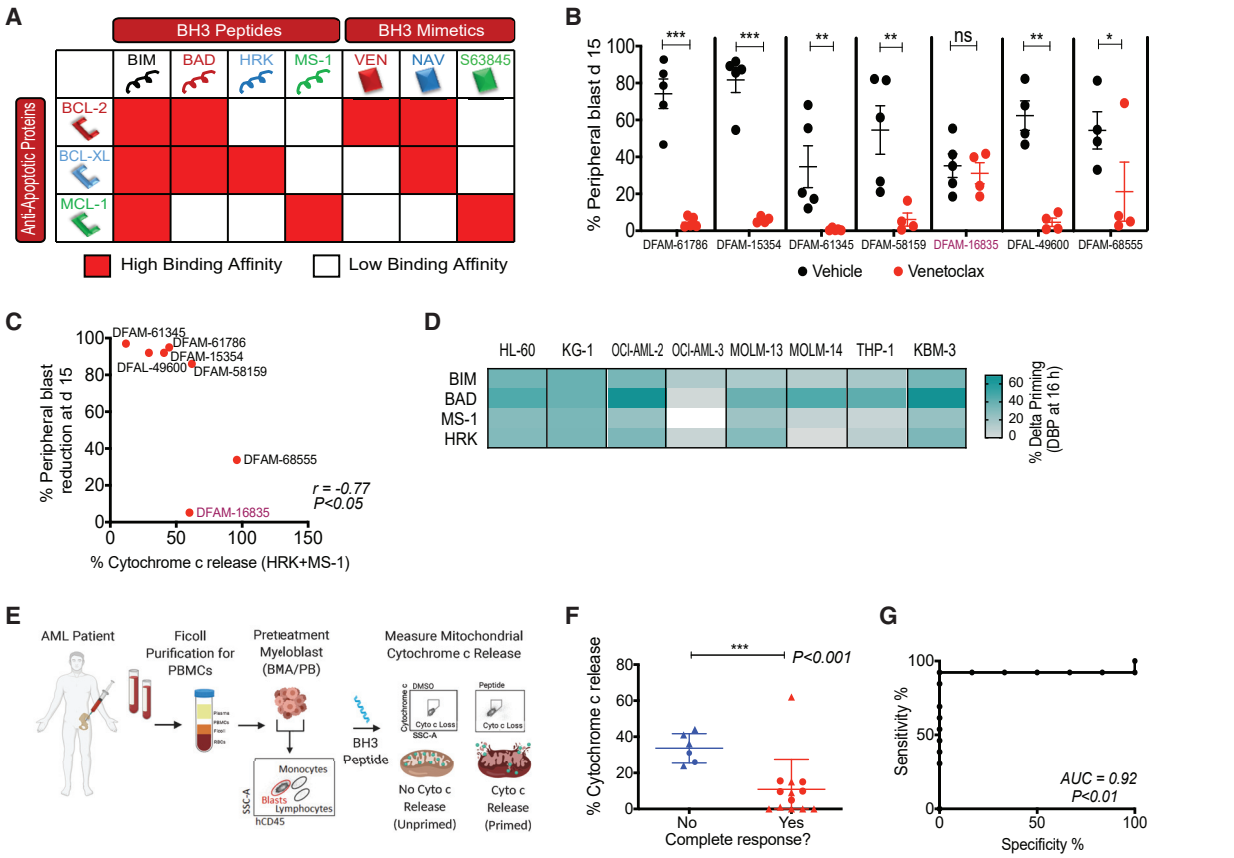

Figure 1. Baseline BH3 Profiling Predicts Clinical Response to Venetoclax and Hypomethylating Agent Combination

(A) Interaction map for BH3 peptides and BH3 mimetics with BCL-2 family proteins. Red, K_d < 100 nM, determined by fluorescence polarization. Ven, venetoclax; Nav, navitoclax.

(B) Percentage of hCD45$^+$ circulating blasts in AML PDXs on venetoclax treatment (100 mg/kg, PO, 5 days/week) for 2 weeks. Mean ± SEM, n = 5 mice; *p < 0.05, **p < 0.01, ***p < 0.001; two-tailed Student's t test.

(C) Spearman correlation between cytochrome *c* release caused by HRK + MS-1 peptides in pretreatment PDX myeloblasts and blast reduction at day 15 after therapy.

(D) Heatmap of delta priming responses to indicated peptides in AML cell lines at 16 h of azacitidine treatment. Delta priming = % cytochrome c loss^{drug} — % cytochrome c loss^{DMSO} (n = 3 replicates).

(E) Schematic of BH3 profiling of AML patient myeloblasts.

(F) Cytochrome *c* release derived from BH3 profiling using HRK + MS-1 peptides in pretreatment myeloblasts compared with response status of patients treated with venetoclax plus HMA. Circles, phase 1b (NCT02203773) clinical trial patients (n = 7); triangles, off-trial patients (n = 12); horizontal line, median with interquartile range; ***p < 0.001; one-tailed Wilcoxon rank-sum test.

(G) Receiver operative characteristic curve of HRK + MS-1-induced cytochrome *c* release versus clinical response.

See also Figure S1 and Tables S1 and S2.

involved the MOM. We derived five new AML PDX models of acquired venetoclax resistance, five PDX models that had responded to venetoclax, and one inherently resistant model (DFAM-16835) as a control (Figure 1C) (Table S1). Leukemia-bearing mice were dosed for 5 days a week with 100 mg/kg venetoclax per gavage until resistance emerged (Figure 2A). This dose resulted in myeloblast reduction to <1% of circulating leukocytes in two of six models (Figure 2B). For each model, we found >90% bone marrow and spleen involvement, as shown by hCD45 surface expression (Figure S2A). All initially sensitive models acquired resistance to venetoclax (Figure 2C). A recent report linked selection for venetoclax resistance in AML to acquisition of a more monocytic phenotype, indicated by an increase is several cell surface markers, including CD11b (Wei et al., 2020). To determine whether venetoclax resistance arises from leukemia stem cells (LSCs) or rather from monocyte/macrophage differentiation, we compared the immunophenotype of parental and resistant myeloblasts. Results were somewhat mixed: two models (DFAM-61786 and DFAM-61345) showed increased expression of LSC markers (CD117$^+$ and CD34$^+$ CD38$^-$) at resistance, while none of the relapsed myeloblasts exhibited a monocytic surface phenotype (CD11b$^+$/CD14$^+$), as indicated in Figure S2B.

Venetoclax Resistance Can Be Observed Independently of Recurrent Mutations in Leukemia-Related Genes

Having established venetoclax-resistant PDX models, we next sought to determine the molecular mechanisms underlying

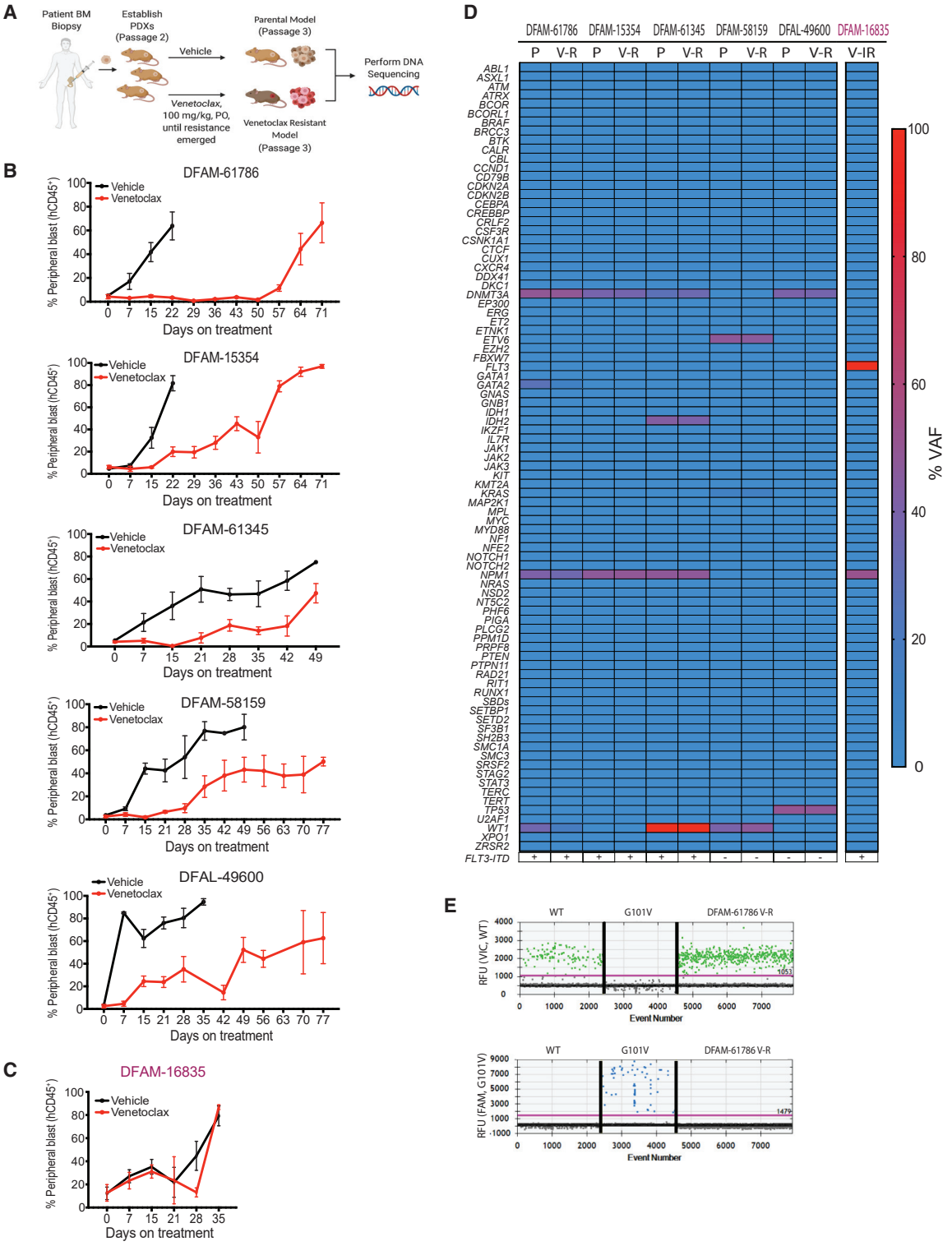

Figure 2. *In Vivo* Resistance to Venetoclax Emerges in the Absence of Genetic Mutations in Known Leukemia Genes

(A) Schematic of *in vivo* venetoclax-resistant models generation.

(B and C) Percentage of hCD45$^+$ circulating blasts after venetoclax or vehicle treatment in indicated PDXs. The models in (B) acquired resistance to venetoclax while the model in (C) was intrinsically resistant. Mean ± SEM, n = 5.

(D) Pairwise comparison of parental and resistant PDX mutation status and variant allele frequency.

(legend continued on next page)

in vivo emergence of resistance. Genetic alterations have been previously identified in venetoclax-resistant CLL patients and *in vitro* AML cell lines and patient samples (DiNardo et al., 2020; Blombery et al., 2019; Nechiporuk et al., 2019). We evaluated pathogenic mutations detected by the rapid heme panel (RHP), which comprises clinical targeted next-generation sequencing and copy number variation analysis for 88 genes recurrently mutated in hematologic malignancies (Kluk et al., 2016). The final variant list revealed a range of three to nine variants per PDX (see Table S1 for details on individual mutations). A comparison of mutational frequencies among parental and resistant PDXs showed no marked differences (Figure 2D). We also searched for the Gly101Val *BCL2* mutation (Blombery et al., 2019), which is not present in the RHP. We did not detect the presence of Gly101Val *BCL2* mutation via digital droplet PCR in six venetoclax-resistant PDXs (one example shown in Figure 2E). Overall, we find that venetoclax resistance in AML can evolve without genomic alterations in clinically relevant leukemia genes or the *BCL2* gene.

Venetoclax-Resistant PDXs Exhibit Reduction in Mitochondrial Apoptotic Priming

Since venetoclax resistance could not be explained by the genetic mutations we examined, we hypothesized that venetoclax resistance could emerge via altered expression and interaction of BCL-2 family proteins. As a summary measurement of alterations of the BCL-2 family at the MOM, we performed baseline (i.e., in the absence of any current drug treatment) BH3 profiling to measure apoptotic priming. In all PDX models of acquired resistance, we found a reduced sensitivity of mitochondria from venetoclax-resistant myeloblasts to BIM, PUMA, and BAD BH3 peptides, as well as to direct mitochondrial exposure to venetoclax (Figures 3A and 3B).

Next we compared mitochondrial priming of paired pretreatment and post-relapse myeloblasts of patients who had a CR followed by a relapse on venetoclax and azacitidine (n = 9) (Figure 3C). In four of these cases, there was intervening allogeneic stem cell therapy while in remission. Although we observed acquisition of new mutations and >15% changes in VAF between paired clinical samples from pretreatment and post-relapse myeloblasts of patients treated with venetoclax and azacitidine, there was no consistent molecular signature that defined a relapsed phenotype (Figure 3D). Notably we observed selection for decreased overall mitochondrial priming in relapsed myeloblasts using promiscuously interacting BIM ($p = 0.0075$) and PUMA peptides ($p = 0.0078$), as shown in Figure 3E. Simultaneously we also observed reduced mitochondrial sensitivity to venetoclax in relapsed samples ($p = 0.02$). With regard to MCL-1 dependence, relapsing myeloblasts displayed mainly persistent rather than increased mitochondrial sensitivity to the MS-1 peptide (two of nine patients showed >15% priming at relapse). There was no significant difference in BCL-XL dependence after relapse. These results suggest that what we observed in the PDX models is clinically relevant—reduced mitochondrial priming is a mechanism of acquired resistance to venetoclax in the clinic.

Venetoclax-Resistant PDXs Exhibit Heterogeneous Changes in BCL-2 Family Protein Expression

To investigate the molecular basis to altered mitochondrial priming, we next measured protein expression patterns of BCL-2 family anti-apoptotic genes in parental and resistant cells from four different PDX models of acquired venetoclax resistance. MCL-1 upregulation has previously been implicated in the development of venetoclax or navitoclax resistance (Yecies et al., 2010). Indeed three of the four acquired resistant PDX models, DFAM-61786, DFAM-15354, and DFAM-58159 had upregulated MCL-1 compared with parental cells (Figures 3F and S3A). Upregulation in BCL-XL was seen in models DFAM-61786 and DFAM-58159. BCL-2 phosphorylation on serine-70 enhances BCL-2's anti-apoptotic function via promoting its binding to BAK (Dai et al., 2013). When normalized to vinculin, none of the four acquired resistance PDXs showed greater than 2-fold change in p-BCL-2 levels (Figure S3A). No decrease was observed in pro-apoptotic BIM, BAD, or NOXA expression in any model. BAX or BAK loss has shown to be associated with decreased apoptosis sensitivity (Sarosiek et al., 2013) and BAX phosphorylation at serine-184 is shown to be associated with BAX inactivation (Kale et al., 2018). However, we observed no changes in p-BAX or total BAX between parental and resistant myeloblasts. Notably, BAK was downregulated in three of the four models of acquired resistance and, in the fourth, BAK protein expression was already low in the parental (Figures 3F and S3A). These results suggest that BAK loss might be a consistent feature of driving venetoclax resistance *in vivo*. Upregulation in mitochondrial chaperone CLPB (Chen et al., 2019) and inactivation of p53 has been reported as a major contributor to venetoclax resistance in AML cell lines (Nechiporuk et al., 2019). We observed increased CLPB protein expression in only one PDX model but increased p53 protein levels (often indicative of p53 inactivation) in three of four models. However, none of these three models showed mutations in p53 at baseline or after acquisition of venetoclax resistance (Figures 3F and 2D; Table S1). A combination of decreased BAK expression and/or increased BCL-XL or MCL-1 expression offers a potential molecular explanation for the reduction in priming we observed.

MCL1:BIM Replace BCL-2:BIM Complexes in Venetoclax-Resistant Myeloblasts *In Vivo*

We hypothesized that in a resistant cell, BCL-2's sequestration of pro-apoptotic proteins, necessary for BCL-2 dependence (Souers et al., 2013; Certo et al., 2006; Del Gaizo Moore et al., 2007) might be reduced. Notably, all four PDXs with acquired resistance tested showed reduced to no binding of BCL-2 to BIM compared with parental cells (Figures 3G and 3H). Since BCL-2 or BIM levels were not decreased after the acquisition of resistance (Figure 3F), the observed difference was attributed

(E) Representative electropherograms for detection of wild-type (WT) (top) and mutant *BCL2* (Gly101Val, bottom) in myeloblasts derived from venetoclax-resistant DFAM-61786 by digital droplet PCR. Top, VIC fluorescence for WT *BCL2* Gly101; Bottom, FAM fluorescence for *BCL2* Gly101Val. Each dot is a droplet; RFU, relative fluorescence unit.
See also Table S1 and Figure S2.

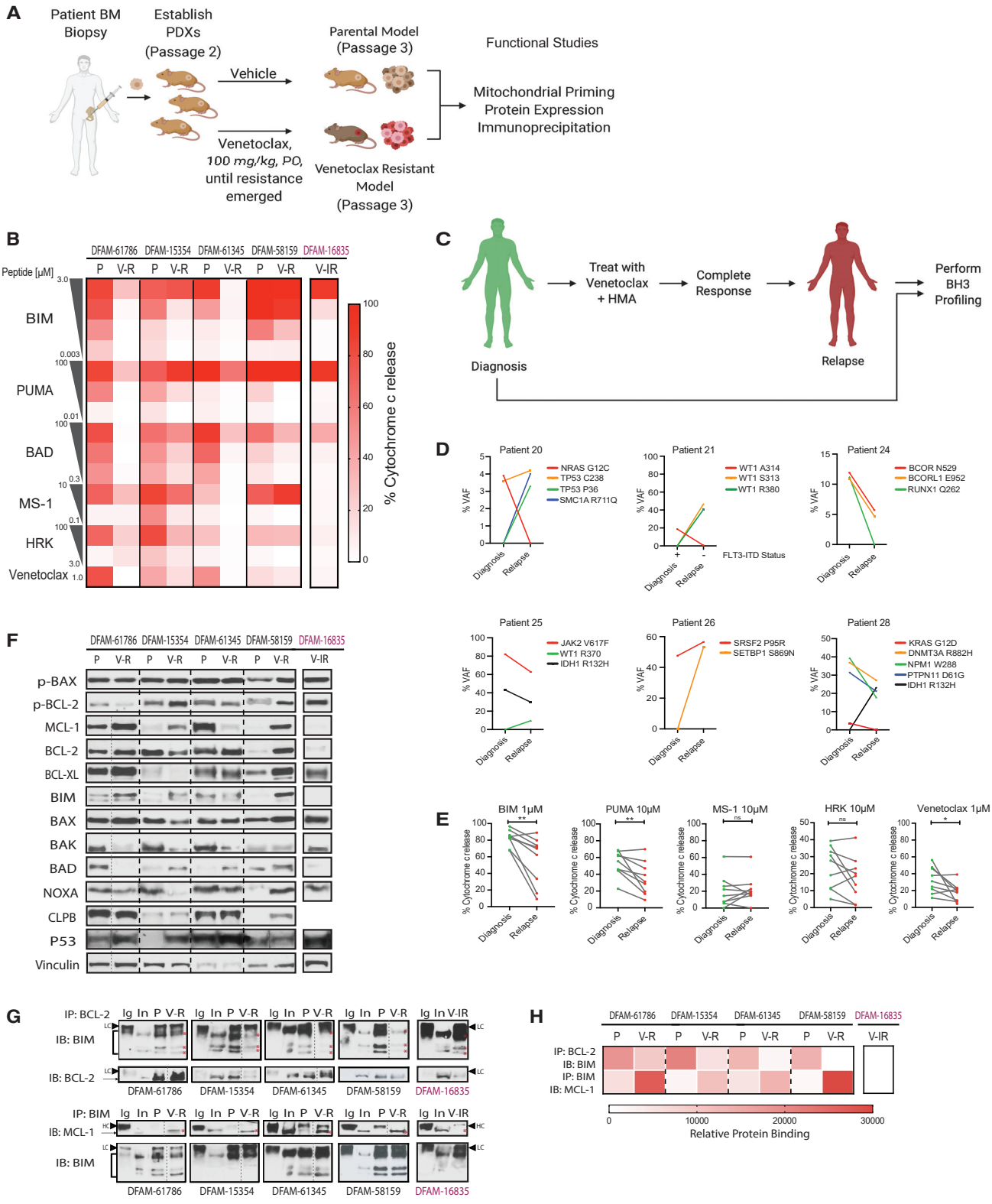

Figure 3. *In-Vivo*-Acquired Resistance to Venetoclax Is Accompanied by Reduction in Mitochondrial Priming and Displacement of BIM from BCL-2 to MCL-1

(A) Schematic of the experimental workflow.

(B) Heatmap of baseline mitochondrial priming in PDXs before and after acquisition of venetoclax resistance (n = 3 mice/group).

(legend continued on next page)

to displacement of BIM from BCL-2 in the resistant samples. To test if an anti-apoptotic protein not targeted by a BCL-2 antagonist might be increasing sequestration of BIM, we immunoprecipitated BIM and then immunoblotted for MCL-1, due to technical difficulty with MCL-1 immunoprecipitation. Strikingly, none of the parental PDXs showed BIM:MCL-1 binding but, upon acquisition of resistance, all four PDXs indicated the presence of BIM:MCL-1 complexes while being treated with venetoclax (Figures 3G and 3H). Intrinsically resistant DFAM-16835 PDX showed no binding between BIM and MCL-1, suggesting that intrinsic resistance may occur via a different mechanism. The increased binding of pro-apoptotic proteins like BIM to MCL-1 provides evidence for a mechanism of resistance based on alterations in the interaction of BCL-2 family proteins at the MOM. Moreover, the loading of MCL-1 with BIM provides a molecular basis for the hypothesis tested below, that MCL-1 antagonism could be effective in the setting of venetoclax resistance. Our BH3 profiling, BCL-2 family protein abundance, and interaction studies are all consistent with an outer mitochondrial membrane-based resistance to venetoclax founded on alterations in BCL-2 family proteins.

DBP Identifies Persistent Drug Sensitivities in Venetoclax Resistance Models

To search for agents that can overcome venetoclax resistance, we isolated myeloblasts from spleens of parental and resistant models, exposed them to a panel of 40 targeted agents *ex vivo* for 16 h, and then performed DBP (Figure 4A). DBP measures induction of apoptotic priming by brief exposures of drugs to cells, and it has been shown to predict *in vivo* efficacy of drugs (Montero et al., 2015). Altered mitochondrial response to the promiscuously interacting BIM BH3 peptide, which interacts with all anti-apoptotic molecules, and which can directly activate BAX and BAK, was used to determine differential drug response. Strikingly, most targeted agents, regardless of mechanism of action, demonstrated a reduced ability to induce apoptotic signaling in venetoclax-resistant cells compared with parental cells (Figure 4B). This suggests that, while venetoclax-specific mechanisms may be involved in venetoclax resistance, broad resistance to anti-cancer agents is observed due to general selection for reduced apoptotic signaling. Nonetheless, a small number of agents induced persistent apoptotic priming responses in both pre- and post-venetoclax-resistant myeloblasts. Treatment with three different selective FLT3 inhibitors (quizartinib, crenolanib, and gilteritinib) primed parental as well as resistant myeloblasts in three acquired resistant models carrying *FLT3-ITD* mutations (DFAM-61786, DFAM-15354, and DFAM-61345). In addition, SMAC mimetics (birinapant and LCL-161), an HDAC inhibitor (panobinostat), MCL-1 antagonists (AZD 5991 and S63845), and a CDK-9 inhibitor (AZD 4573, thought to operate by indirectly reducing MCL-1 levels) (Cidado et al., 2020) maintained the ability to induce apoptotic priming even after the acquisition of venetoclax resistance (Figures 4B and S3B).

Given the clinical relevance of azacitidine, we specifically queried if venetoclax resistance affects the ability of azacitidine to induce mitochondrial priming. As measured by the BIM peptide, azacitidine-induced priming increased in acquired resistant DFAM-61786, but decreased in acquired resistant DFAM-15354, DFAM-61345, and DFAM-58159 (Figure 4C). In parental cells, there is a consistent pattern of azacitidine enhancing mitochondrial sensitivity to the BAD BH3 peptide. This enhancement, however, decreases in the models of acquired venetoclax resistance (Figure 4C). Finally, we confirmed in patient myeloblasts that relapsed after clinical treatment with venetoclax + HMA that venetoclax sensitivity was dramatically reduced at relapse while quizartinib, S63845, AZD4573, and birinapant demonstrated persistent mitochondrial priming (Figures 4D and 4E). This suggests that the drugs identified by DBP in venetoclax-resistant AML PDXs may be relevant to human clinical venetoclax resistance also.

BCL-2 and MCL-1 Antagonists Displace Pro-apoptotic Proteins from Drug-Targeted to Non-targeted Anti-apoptotic Proteins

The human clinical examples, DBP, and protein interaction studies above suggested that venetoclax could cause displacement of pro-apoptotic proteins from BCL-2 to MCL-1 in myeloblasts, and that venetoclax-resistant myeloblasts might maintain sensitivity to MCl-1 antagonists. To better address mechanisms of combination use of BCL-2 and MCL-1 antagonists, we first turned to DBP of seven AML cell lines and verified that each BH3 mimetic individually increased overall apoptotic priming, as measured by the promiscuous BIM BH3 peptide in all cell lines (Figures 5A and 5B). As expected from our displacement studies, venetoclax resulted in an increase in mitochondrial MCL-1 dependence indicated by response to MS-1 peptide in MOLM-13, KG-1, OCI-AML-2, OCI-AML-3, and HL-60 cells (Figure 5A). In contrast, S63845 treatment increased mitochondrial BCL-2 dependence as measured by the BAD BH3 peptides and mitochondrial sensitivity to venetoclax in all cell lines (Figure 5B). These results suggest that increased myeloblast mitochondrial sensitivity to BAD BH3 and MS-1 BH3 can serve as pharmacodynamic markers for S63845 and venetoclax therapy, respectively.

We then investigated kinetics of mitochondrial changes following BH3 mimetic exposure. Increase in MCL-1 dependence by venetoclax and BCL-2 dependence by S63845 was

(C) Schematic of pair wise BH3 profiling in AML patients.

(D and E) Pairwise comparisons of (D) mutation status and variant allele frequency and (E) cytochrome *c* release using the indicated peptides in AML patient samples at diagnosis and at relapse on VEN + AZA (n = 9 pairs). Each dot represents mean of three replicates; *$p < 0.05$, **$p < 0.01$; two-tailed Student's t test.

(F) Immunoblotting (IB) for BCL-2 family proteins in parental and venetoclax-resistant PDX myeloblasts. Fine dashed lines indicate fusion between two lanes from the same gel. Longer dashed lines indicate distinct gels.

(G and H) (G) Immunoprecipitation (IP) for BCL-2 followed by IB for BIM (top). IP of BIM followed by IB for MCL-1 (bottom). red*, correct band size for proteins; HC, IgG heavy chain; LC, IgG light chain. (H) Heatmap for corresponding densitometry using ImageJ. Fine dashed lines indicate fusion between two lanes from the same gel. P, parental; V-R, venetoclax-acquired resistance; V-IR, venetoclax-intrinsic resistance.

See also Table S1 and Figure S3.

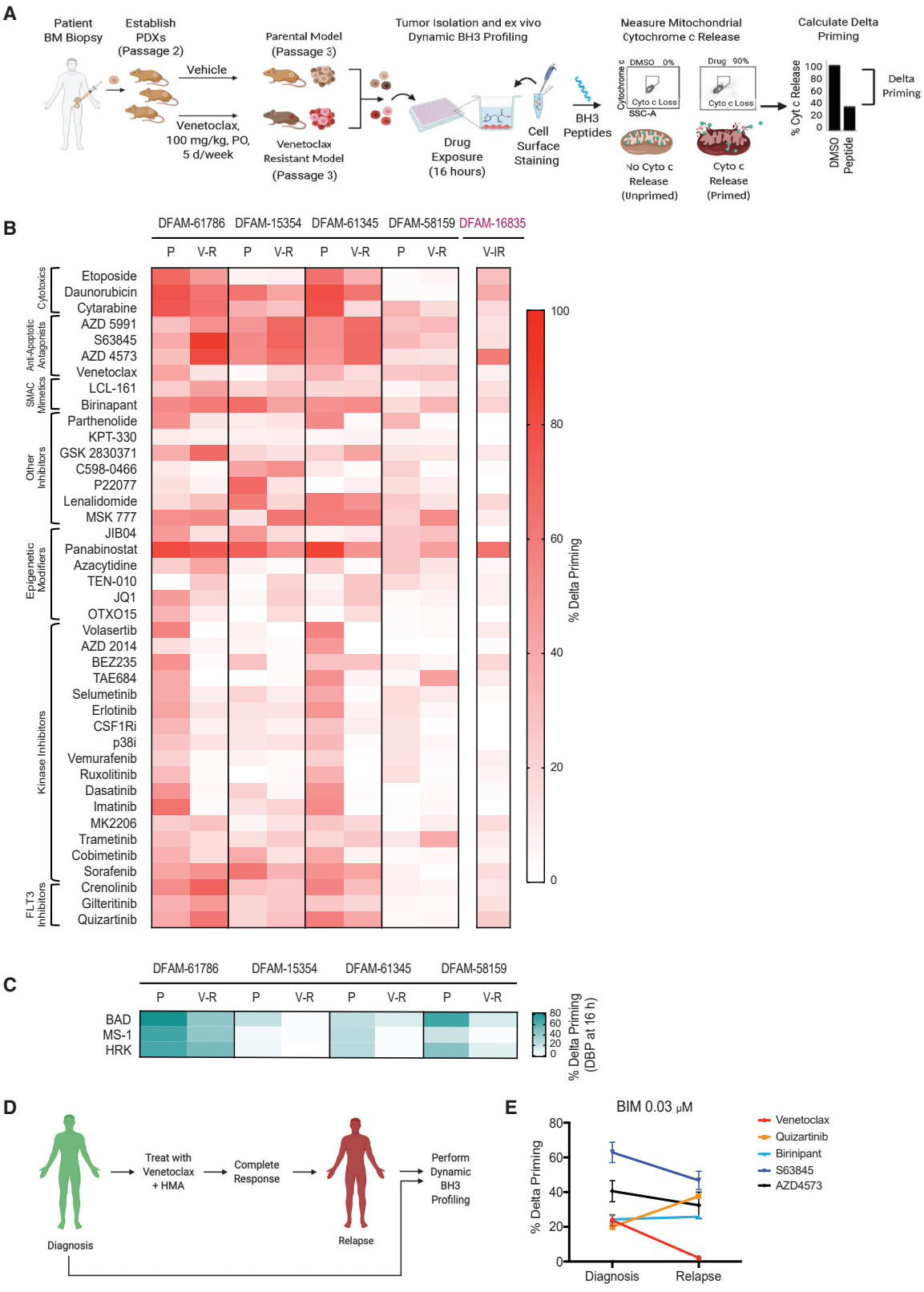

(legend on next page)

observed within 1 h of treatment of MOLM-13 cells, consistent with rapid displacement of pro-apoptotic proteins from BCL-2 to MCL-1 (Figures 5C and 5D). While changes in mRNA levels of some BCL-2 family members was observed, except for MCL-1 upregulation in response to S63845, protein levels of other BCL-2 family members were not significantly altered (Figure S4). MCL-1 transcript and protein increases following venetoclax treatment may therefore offer a partial explanation of enhanced MCL-1 dependence. However, changes in BCL-2 dependence following S63845 treatment are not explained by changes in protein and transcript levels. Nonetheless, these results leave open the possibility of rapid displacement of pro-apoptotic proteins from drug-targeted to non-targeted anti-apoptotic proteins at the mitochondrion.

We next performed co-immunoprecipitation assays to test for displacement of BIM from targeted to non-targeted anti-apoptotic proteins. Venetoclax caused a shift in BIM from BCL-2 to MCL-1, providing the basis for the increased mitochondrial sensitivity to MS-1 (Figure 5E). Of note, S63845 treatment resulted in displacement of MCL-1 from NOXA as an indication of pharmacodynamic activity of S63845 (Figure 5E). These results are consistent with displacement of pro-apoptotic proteins from the targeted anti-apoptotic target of BH3 mimetic drugs as an explanation for a rapid shift in anti-apoptotic dependence in AML, similar to other contexts (Matulis et al., 2016; Morales et al., 2011).

BCL-2 and MCL-1 Antagonism Is Synergistic *In Vitro* and *In Vivo*

Our results led us to hypothesize that shifts in binding and dependencies would explain reported synergy between BCL-2 and MCL-1 antagonists. We first validated synergy between venetoclax and S63845 combination in a panel of AML cell lines (Figure 5F), in agreement with earlier studies (Ramsey et al., 2018; Caenepeel et al., 2018; Tron et al., 2018). If our mitochondrial hypothesis is correct, then BH3 mimetic synergy should mirrored by DBP. We calculated the sum of delta priming response to BAD and MS-1 peptides after individual treatment with S63845 and venetoclax, respectively, which was a good predictor of synergy between BH3 mimetics as determined by the Loewe synergy score (Figure 5G; Spearman $r = 0.77$, $p < 0.05$). This suggests that the mechanism of synergy lies in interactions of BCL-2 family proteins in the MOM. Moreover, mitochondrial BH3 profiling can provide a rapid pharmacodynamic marker for predicting response to BH3 mimetic combinations as well as to single agents.

After establishing an effective and tolerable dosing regimen, the parental, venetoclax-sensitive AML PDX model DFAM-61786 was treated with either venetoclax (50 mg/kg), S63845 (25 mg/kg), or both drugs. Combination treatment resulted in reduction of circulating myeloblasts greater than either single agent (Figure 5H). As expected, these results demonstrate *in vivo* efficacy with combined BCL-2 and MCL-1 inhibition.

Combination BCL-2 + MCL-1 Antagonism Has Anti-leukemic Activity Despite Acquired Venetoclax Resistance

We next tested whether MCL-1 inhibition is efficacious in the setting of venetoclax resistance. We generated a venetoclax-resistant MOLM-13 AML cell line by long-term selection in slowly escalating concentration of venetoclax up to 2,000 nM (Figure S4D). As in the venetoclax-sensitive context, BCL-2 + MCL-1 inhibition is superior to single-agent MCL-1 inhibition, here using the clinical analog of S63845, MIK665 (Figure 6A). Of note, venetoclax-resistant MOLM-13 cells also showed upregulation in MCL-1 and loss in BAX (Figure S4E).

Next we measured S63845 efficacy in acquired venetoclax-resistant PDX models DFAM-61786, DFAM-61345, and DFAM-15354 (all three with high BIM:MCL-1 binding) and intrinsic venetoclax-resistant DFAM-16835 (no BIM:MCL-1 binding). Modest initial sensitivity to venetoclax monotherapy in two models (DFAM-15354 and DFAM-61345) might be attributed to the drug holiday 4 weeks after serial transplantation (Figures 6B and 6C). S63845 monotherapy resulted in significant myeloblast reduction in only venetoclax-resistant DFAM-15354 ($p < 0.05$) (Figure 6C). This suggested that S63845 monotherapy provided a moderate advantage compared with vehicle in venetoclax-resistant models. As expected, S63845 had no efficacy in the intrinsically resistant DFAM-16835 model.

Our previous results suggest that treatment with venetoclax would enhance MCL-1 dependence. We next tested if the combination of venetoclax and S63845 outperformed monotherapy in the setting of *in vivo* venetoclax resistance. Of note, combining the highest tolerable single-agent doses (100 mg/kg venetoclax and 40 mg/kg S63845) led to sudden death in three of five mice within 24 h of the first dose Figure S5A. We found that this toxicity was largely, although not completely, dependent on the presence of myeloblasts, raising the possibility of tumor lysis syndrome, further explored in Figures S5B and S5C. Note that our study was not designed to be a definitive model of toxicity, as S63845 binds murine MCL-1 with less affinity that human MCL-1 (Kotschy et al., 2016).

To investigate if alternating BCL-2 and MCL-1 antagonist treatment might represent a practical strategy to improve therapeutic index, we tested five different combination schemes (Figure 6D). We first tested combinations 1 to 3 in which venetoclax and S63845 were not dosed on the same day to reduce overlapping toxicity. Although all combination treatments showed better

Figure 4. Dynamic BH3 Profiling Identifies Drug Vulnerabilities in *In Vivo* Venetoclax-Resistant AML

(A) Schematic of dynamic BH3 profiling (DBP).

(B and C) Heatmap of DBP results comparing delta priming responses in the myeloblasts derived from parental and venetoclax-resistant PDXs at 16 h drug treatment. Delta priming response to (B) 40 targeted agents and to (C) azacitidine. Each result reflects three independent mice as biological replicates of two technical replicates each.

(D) Schematic of pairwise DBP in single AML patient.

(E) Comparison of delta priming response to BIM peptide in patient myeloblasts at diagnosis and relapse on VEN + AZA at 16 h treatment with indicated drugs. Mean ± SD, n = 3.

See also Figure S3.

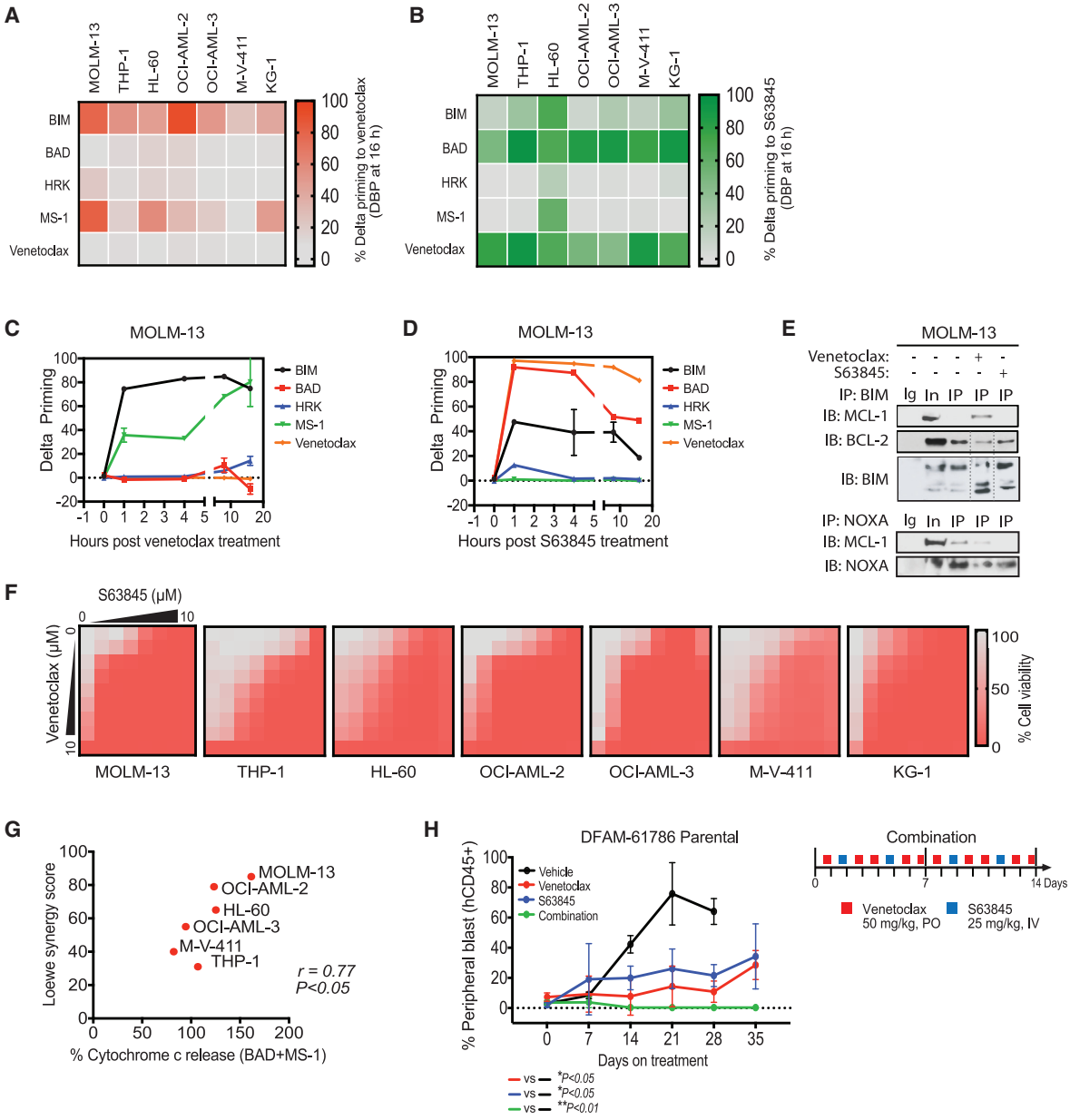

Figure 5. Mitochondrial Sensitivities to BH3 Peptides Reveal Basis for Synergy between BH3 Mimetics

(A and B) Heatmap of delta priming response in AML cell lines after treatment with (A) 5 nM venetoclax and (B) 50 nM S63845 for 16 h, determined by dynamic BH3 profiling (n = 3).

(C and D) Delta priming kinetics of MOLM-13 cell line after treatment with (C) venetoclax and (D) S63845. Mean ± SD, n = 3.

(E) IP of BIM in MOLM-13 cell line to detect binding with MCL-1 and BCL-2 following 1 h treatment with venetoclax and S63845. Fine dashed lines indicate fusion between two lanes from the same gel.

(F) Cell viability heatmap of indicated AML cell lines at 24 h treatment with venetoclax and S63845 (n = 3).

(G) Spearman correlation between Loewe synergy score for venetoclax and S63845 combination and delta priming response to BAD + MS-1 peptides shown in (A and B).

(H) Percentage of hCD45$^+$ leukemic cells in AML PDX subjected to venetoclax (50 mg/kg, p.o., 5 days/week), S63845 (25 mg/kg, i.v., 2 days/week), or combination. Mean ± SEM, n = 5 mice; *p < 0.05, **p < 0.01; one-way ANOVA.

See also Figure S4.

efficacy compared with monotherapy, mice that received venetoclax and S63845 in the same week (combination 1) showed the greatest anti-leukemic activity (Figure 6E). We therefore next tested concurrent BH3 mimetic treatment in combinations 4 and 5, where mice received venetoclax consecutively on days 1–5 and 8–12. In combination 4, S63845 was given from the

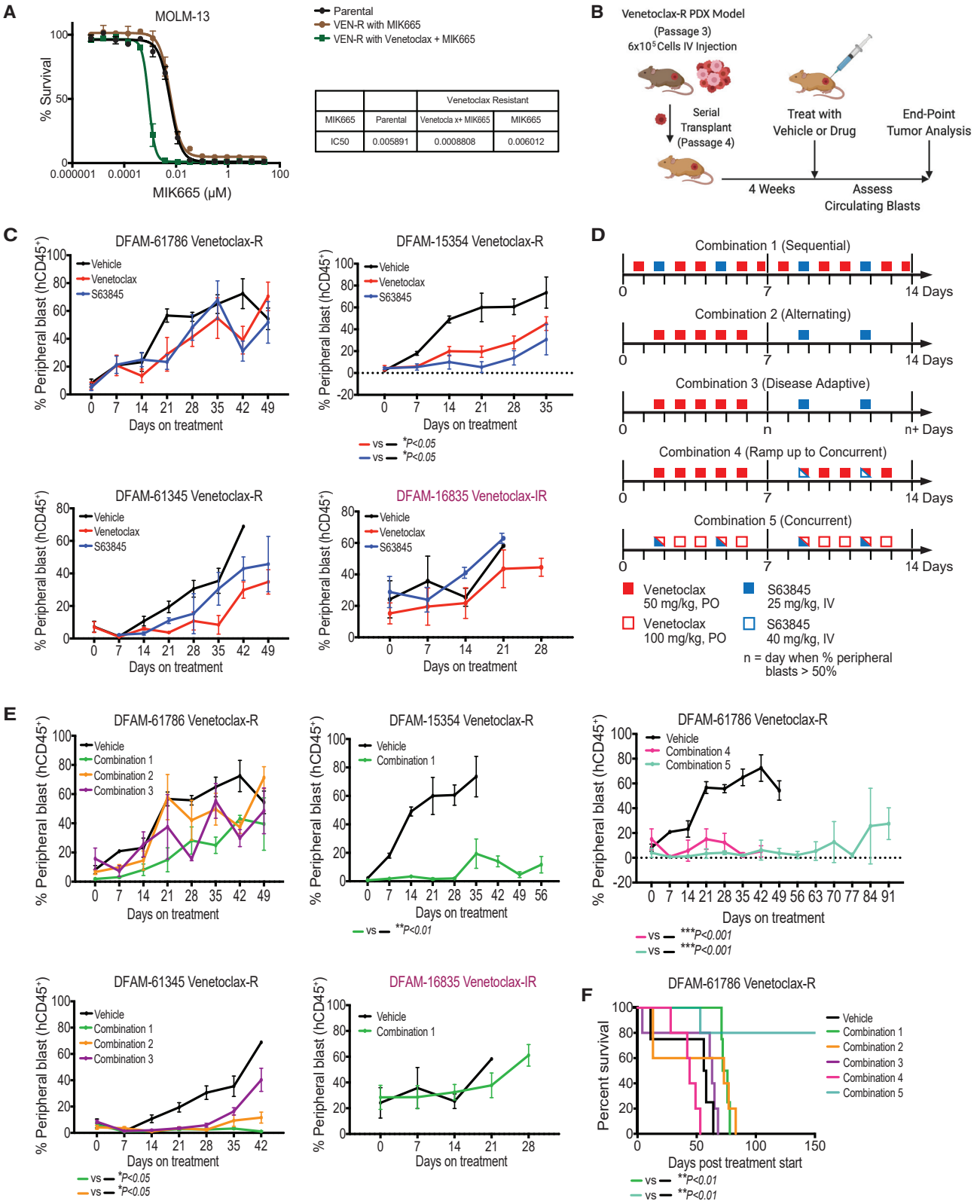

Figure 6. Dual Targeting of BCL-2 and MCL-1 Inhibits Leukemia Progression of Venetoclax-Resistant PDX Models

(A) Cell viability of parental and venetoclax-resistant MOLM-13 cells treated with MIK665 and ±1.3 μM venetoclax at 72 h. Mean ± SEM, n = 2.

(B) Schematic of PDX treatment, n = 5 mice/arm.

(legend continued on next page)

second week on days 8 and 11 while in combination 5, S63845 was started from the first week itself on days 1, 4, 8, and 11. Indeed, when animals were treated with both BH3 mimetics on the same day we observed maximal regression to <5% of circulating leukocytes in all mice (Figure 6F). However, combination 4 was least tolerable at doses of S63845 at 40 mg/kg, while combination 5 provided the greatest survival advantage among all five treatment combination schedules (Figure 6G). We concluded that simultaneous antagonism of BCL-2 and MCL-1 has efficacy superior to that of sequential antagonism, or single-agent therapy, consistent with mechanistic synergy. While individually each drug displaces pro-apoptotic proteins from its targeted protein to the non-targeted protein, maintaining survival, the combination of drugs blocks escape of leukemic cells because pro-apoptotic protein sequestration is prevented simultaneously in BCL-2 and MCL-1.

FLT3 Inhibitors and SMAC Mimetics Reduces Leukemia Burden in Venetoclax-Resistant PDX Models

We next asked if DBP can identify agents other than MCL-1 antagonists active in venetoclax-resistant AML. We found in parental models that were primed by FLT3 inhibition (DFAM-61786, DFAM-15354, and DFAM-61345) and SMAC mimetics (DFAM-61786, DFAM-15354, DFAM-61345, and DFAM-58159), that apoptotic priming response persisted after venetoclax resistance (Figure 4B). While delta priming was not generally increased in the resistance models for these drugs, the persistence of delta priming indicated that these drugs could induce apoptotic signaling even in the venetoclax-resistant state. Persistent activity was characterized as >15% delta priming response to drugs after acquisition of venetoclax resistance (derived from the mean of 3 SD of DMSO-treated wells). Note that, consistent with these results, others have found that FLT3 signaling persists or even increases on acquisition of resistance to venetoclax (DiNardo et al., 2020).

To validate DBP results *in vivo*, NSG mice transplanted with parental and venetoclax-resistant myeloblasts from FLT3-mutated PDX models DFAM-61786 and DFAM-15354 were subjected to quizartinib, birinapant, and LCL-161 *in vivo* treatment. In comparison with vehicle treatment, quizartinib delayed progression (Figure 7A, 41 versus >300 days) and prolonged median survival (60 versus >300 days) in the DFAM-61786 venetoclax-resistant model. Compartmental analysis at 310 days showed significant reduction in myeloblasts across the spleen, bone marrow, and PB in the venetoclax-resistant DFAM-61786 model (Figure 7B). Near-total elimination of circulating myeloblasts was also observed in DFAM-15354 (Figure 7C). As we had predicted from DBP results, sensitivity of venetoclax-resistant PDXs to FLT3 inhibition was comparable with their parental counterparts (Figures 7A and 7C), although improved survival was observed in venetoclax resistant over parental DFAM-61786 treated with quizartinib ($p < 0.01$). Of note, prolonged treatment with quizartinib showed no signs of toxicity measured via histological analysis using H&E staining of major organs, such as the heart, lungs, liver, and kidney (data not shown).

Next, we compared the *in vivo* efficacy of IAP antagonists (SMAC mimetics) to overcome venetoclax resistance. Although both birinapant and LCL-161 delayed progression in the setting of venetoclax resistance, birinapant, a bivalent SMAC mimetic, showed greater efficacy in models DFAM-61786 and DFAM-15354 (Figures 7D and 7E). We confirmed that both drugs reduced cIAP-1 protein levels as reported previously (Condon et al., 2014) while having no effect on XIAP levels in AML cell lines (Figure S6A). cIAP-1 expression was detectable in venetoclax-resistant PDX models (Figure 7F). Mitochondrial measurements by DBP at 16 h therefore identified SMAC mimetics and FLT3 inhibitors as potential therapies for venetoclax-resistant AML PDX models. When we attempted similar identification by conventional cytotoxic assays on primary myeloblasts, quizartinib and gilteritinib resulted in minimal cell killing in both parental and resistant myeloblasts at 24 h, while extended culture beyond 24 h resulted in high background spontaneous cell death (Figure S6B). This suggests an advantage of DBP when drug-induced cell death takes longer than 24 h, as is the case with many drugs.

We next characterized the mechanism of persistent quizartinib sensitivity in venetoclax-resistant PDXs. Using PCR-based identification of internal tandem duplications (ITD) of the FLT3 gene we found that venetoclax treatment failed to eliminate ITD-bearing subclones. We did not detect any new mutations in *FLT3* (Figure 2D; Table S1). FLT3 signaling can potentially propagate via three distinct downstream proteins, STAT5, MAPK, and PI3K/AKT (Takahashi, 2011). Acquisition of resistance to venetoclax was accompanied by increased signaling, as measured by phosphorylation, in all three arms in DFAM-61786 and DFAM-58159 (Figure 7F). *Ex vivo* quizartinib treatment efficiently decreased FLT3 and STAT5 phosphorylation in DFAM-61786 (Figure 7G). DFAM-61345 showed only increase in pAKT, while DFAM-15354 had a slight increase in pSTAT5 upon venetoclax resistance. While these results suggest there is often selection for enhanced signaling downstream of FLT3 as an explanation of persistent activity of FLT3 inhibitors, we cannot rule out that inhibition of non-FLT3 kinases targeted by quizartinib might also play a role (Zarrinkar et al., 2009).

We also performed gene set enrichment analysis following bulk RNA sequencing of spleen and bone marrow cells collected before and after venetoclax resistance from PDXs DFAM-61786,

(C) Percentage of $hCD45^+$ leukemic cell burden after treatment with single-agent venetoclax (100 mg/kg, p.o., 5 days/week) or S63845 (25 mg/kg, i.v., 2 days/week) or vehicle. Mean ± SEM, n = 5 mice.

(D) Schematics of five different combination regimens for venetoclax and S63845. In combination 3 group ("disease adaptive") switch between treatments was made on the nth day once circulating myeloblasts reached 50%.

(E) Percentage of $hCD45^+$ leukemic cell burden of PDXs in response to five different combination treatment strategies shown in (D). Mean ± SEM, n = 5 mice; $^*p < 0.05$, $^{**}p < 0.01$; one-way ANOVA.

(F) Kaplan-Meier curves showing *in vivo* efficacy of five different combination regimen in venetoclax-resistant DFAM-61786 model. $^*p < 0.05$, $^{**}p < 0.01$; log rank test.

See also Figures S4 and S5.

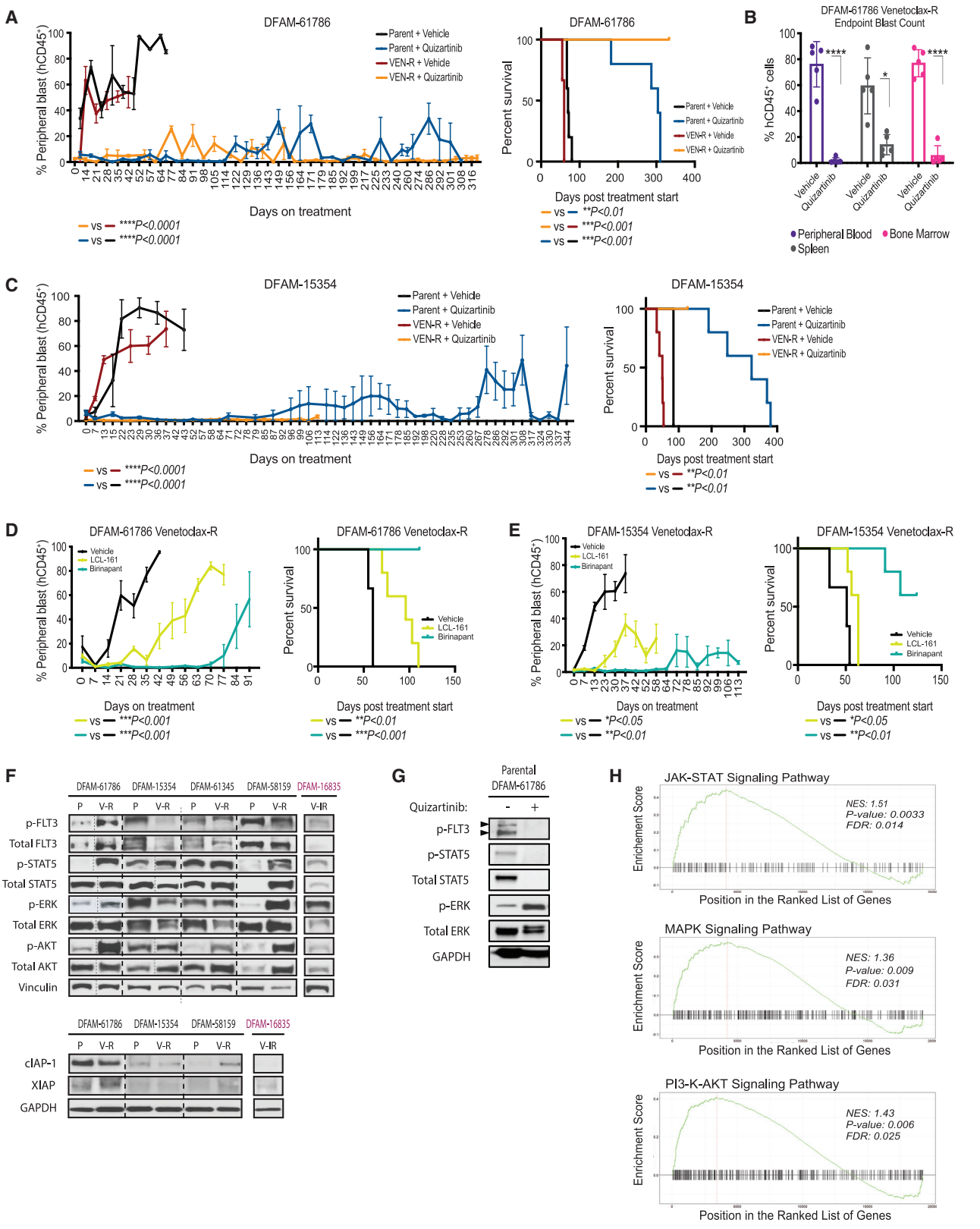

Figure 7. Dynamic BH3 Profiling Identified FLT3 Inhibition and IAP Inhibition as an Effective Strategy in Venetoclax-Resistant Settings

(A–C) Parental or venetoclax-resistant myeloblasts from indicated PDXs were serially transplanted into NSG mice and assigned into treatment arms after 4 weeks post-transplant. (A and C) Percentage of hCD45$^+$ peripheral blast count and corresponding survival curves in response to quizartinib. (B) Percentage of hCD45$^+$

(legend continued on next page)

DFAM-15354, and DFAM-61345. All three venetoclax-resistant PDXs tested depicted enrichment for JAK-STAT, MAPK, and PI3K/AKT pathways (Figure 7H). We also noted enrichment of multiple signatures corresponding to hematopoietic cell lineage, calcium signaling, proteoglycan signaling, and senescence (Figures S7A and S7B). We did not find a transcriptional signature depicting reduction in pro-apoptotic genes and upregulation in anti-apoptotic genes (Figures S7C and S7D). Collectively, our data suggest that venetoclax-resistant myeloblasts acquire reduced apoptotic priming, rendering them resistant to many classes of drugs. This is apparently accompanied by persistent or increased mitogenic signaling, perhaps via upstream tyrosine kinases, which may be responsible for persistent FLT3 inhibitor activity even in the setting of reduced mitochondrial priming.

Myeloblasts Resistant to MCL-1 Antagonism Are Sensitive to BCL-2 Inhibition and FLT3 Inhibition

Our studies on *in vivo* resistance to venetoclax prompted us to ask whether selection for reduced mitochondrial apoptotic priming was a more general property of acquired resistance to BH3 mimetics targeting other anti-apoptotic proteins. To test this, engrafted DFAM-61786 and DFAM-15354 mice were continuously treated with MCL-1 antagonist S63845 (25 mg/kg, i.v., twice a week) until leukemia progressed to create S63845 *in vivo* resistance models (S63-R) (Figures 8A and 8B). Similar to acquired resistance models of venetoclax (Figure 2A) *in vivo* S63-R resistance models (DFAM-61786 and DFAM-15354) also showed decrease in overall mitochondrial apoptotic priming, as shown by reduced mitochondrial sensitivity to BIM and PUMA peptides (Figure 8C). There is also reduced mitochondrial sensitivity to the MCL-1-specific MS-1 peptide, and increased sensitivity to the BAD peptide (Figure 8C).

We performed DBP on S63845-resistant DFAM-61786 and DFAM-15354 myeloblasts to identify drugs that might overcome resistance to MCL-1 antagonism. Targeted agents, including venetoclax, SMAC mimetics, MAPK inhibitors, a JAK2 inhibitor, and tyrosine kinase inhibitors showed persistent priming in resistant myeloblasts (Figures 8D and S8A).

We compared the efficacy of venetoclax as a single agent with that in combination with S63845. Mice receiving venetoclax or the combination exhibited reduced leukemia burden and increased survival benefit, exceeding the therapeutic effect achieved with S63845 and vehicle (Figure 8E). Dual inhibition was not superior to single-agent BCL-2 inhibition in the S63845-resistant model. The FLT3 inhibitor quizartinib, which also caused persistent apoptotic signaling in the S63845-resistant models, caused near-total elimination of circulating myeloblasts in S63-R DFAM-61786 mice up to 63 days and prolonged survival up to 90 days with <5% leukemic blasts in spleen and bone marrow (Figures 8F and 8G). Analogously to the venetoclax-resistant model, we found enhanced activation of the FLT3 pathway (pFLT3) and its downstream targets pSTAT5, pAKT, and pMAPK in S63845-resistant cells compared with parental cells (Figures S8B and S8C). This suggests that acquisition of resistance to MCL-1 and BCL-2 inhibition may share selection for common signaling mechanisms.

DISCUSSION

Targeting BCL-2 has proven to be a major advance in treating AML. Understanding mechanisms of resistance and identifying treatment strategies in the context of acquired resistance to venetoclax hence has become of great importance. Our studies of acquired resistance to venetoclax *in vivo* in PDX models offered not only the ability to identify mechanisms of resistance in a human tumor model, but also the opportunity to compare several different *in vivo* therapeutic strategies, an opportunity not available in other models.

We found that mechanisms of resistance and sensitivity are based in the BCL-2 family at the outer mitochondrial membrane. Most importantly, we consistently found that decreased mitochondrial apoptotic priming accompanies acquired resistance to either BCL-2 or MCL-1 antagonists. This resulted not only in resistance to the BH3 mimetic, but also broadly to resistance to most drugs. We also consistently found that loss of myeloblast sensitivity to venetoclax was accompanied by a loss of direct mitochondrial sensitivity to MOMP induced by venetoclax. As we had previously shown in the context of single-agent venetoclax treatment, BH3 profiling of mitochondria could discriminate responders and non-responders to the venetoclax and azacitidine combination. Such a predictive biomarker might prove of great clinical utility in patients with lower response rates to the combination, such as those with *TP53* mutations or those who have relapsed or refractory leukemia (DiNardo et al., 2019).

Regarding specific molecular mechanisms, we see heterogeneity across our models, and we would anticipate similar heterogeneity in clinical examples within AML, and certainly across different diseases. While specific changes in protein expression differ among models, reduced mitochondrial priming at least partly had its basis in decreased expression of BAK and/or increased expression of BCL-XL and/or MCL-1 in all models with acquired resistance to venetoclax. In addition, there were alterations in BCL-2 family protein complex formation, with a shift from BCL-2:BIM complexes to MCL-1:BIM complexes as resistance to venetoclax was acquired.

Several recent reports have implicated roles for BCL-2 antagonism in various metabolic effects, including mitochondrial energy metabolism, that occur largely on the inner

blast reduction across different compartments upon quizartinib treatment. Mean ± SEM, n = 5 mice; *p < 0.05, **p < 0.01, ***p < 0.001; one-way ANOVA. Survival curve analysis; log rank test. In (C), VEN-R + quizartinib arm study was stopped before endpoint reached due to COVID.

(D and E) Percentage of hCD45$^+$ peripheral blast count and survival curves in response to SMAC mimetics birinapant (25 mg/kg, i.p., 3 days/week) and LCL-161 (100 mg/kg 4 days/week, p.o. Mean ± SEM, n = 5 mice; *p < 0.05, **p < 0.01; one-way ANOVA. Survival curve analysis, *p < 0.05, **p < 0.01; log rank test.

(F) Immunoblots measuring levels of downstream effectors of FLT3 and SMAC mimetic targets in venetoclax-resistant PDXs. Fine dashed lines indicate fusion between two lanes from the same gel. Longer dashed lines indicate distinct gels.

(G) Immunoblots measuring inhibition of FLT3 targets with *ex vivo* quizartinib treatment at 4 h in parental DFAM-61786.

(H) Gene set enrichment analysis showing overlaps of enrichment for JAK-STAT and FLT3/MAPK/PI3K pathway signatures in three different venetoclax-resistant PDXs (61786, 15354, and 61345) compared with parent counterparts. NES, normalized enrichment score; FDR, false discovery rate.

See also Figures S6 and S7.

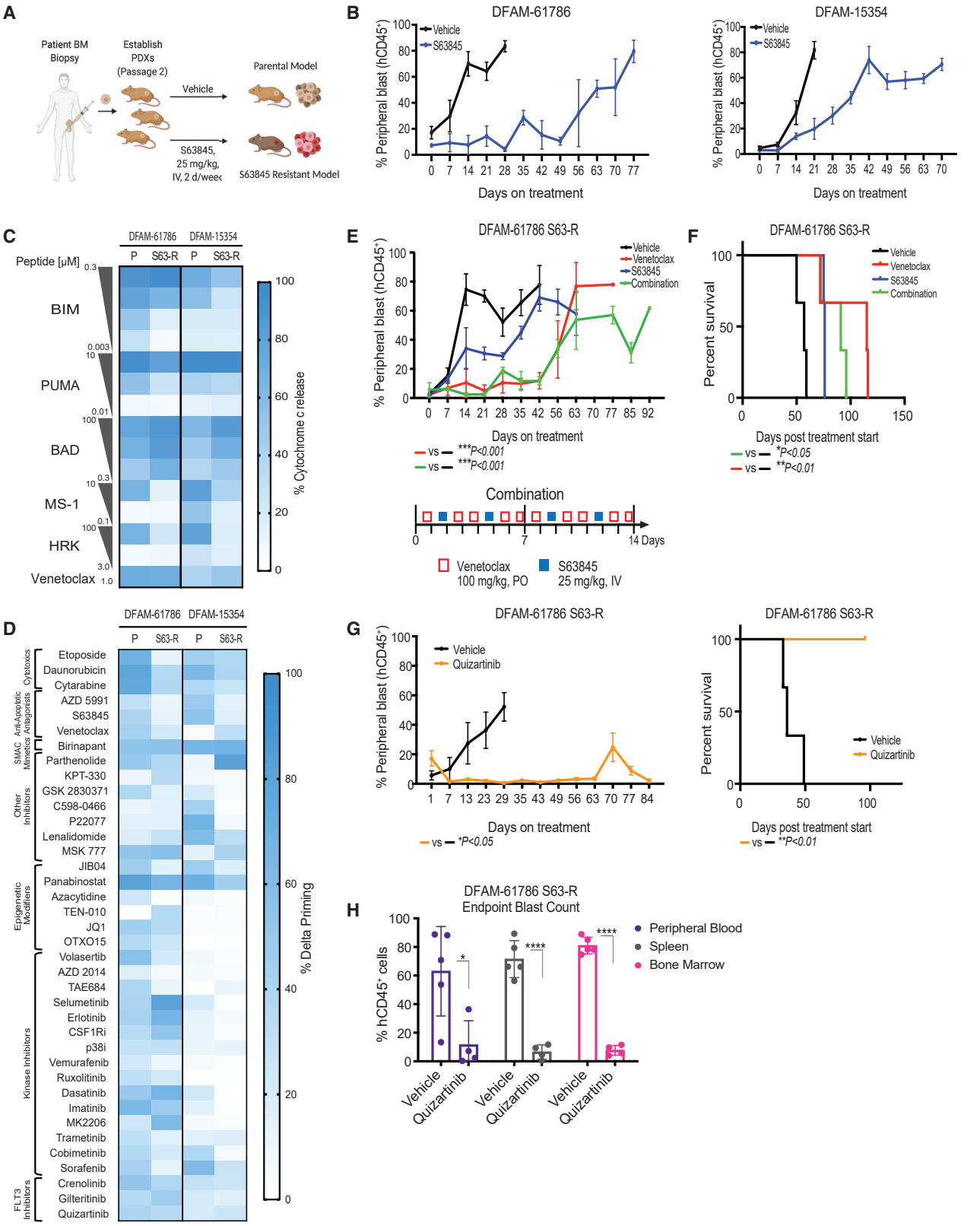

Figure 8. Dynamic BH3 Profiling Identified BCL-2 Antagonism and FLT3 Inhibition as an Effective Strategy in S63845-Resistant Settings

(A) Schematic of modeling of *in vivo* S63845 resistance in AML PDXs.

(B) Leukemic burden in indicated PDX models treated with S63845 (25 mg/kg, i.v., 2 days/week) or vehicle treatment. Mean ± SEM, n = 5 mice.

(legend continued on next page)

mitochondrial membrane (Nechiporuk et al., 2019; Chen et al., 2019; Sharon et al., 2019; Guieze et al., 2019; Pollyea et al., 2018). By performing BH3 profiling and BCL-2 family protein interactions, we provided both accurate prediction and a mechanistic explanation for sensitivity and resistance to BCL-2 and MCL-1 antagonism, based purely on the MOM. While our studies were not designed to rule out effects of BCL-2 antagonism on metabolism, we did not have to consider such effects in predicting and understanding response. Recent work has indicated that, while venetoclax may influence metabolism at higher concentrations, this effect is independent of interaction with BCL-2, and thus is "off-target" (Roca-Portoles et al., 2020). One important point is that on-target BCL-2 antagonism rapidly disrupts electron transport chain (ETC) metabolism at the inner mitochondrion membrane *after* MOMP (Ricci et al., 2003; Waterhouse et al., 2001). Therefore, defects in energy metabolism are to be expected after successful venetoclax therapy, but MOMP may well still be the initiating event. Indeed, the cell death field has long used the loss of potential across the inner mitochondrial membrane as a surrogate for MOMP via dyes like JC-1 and TMRE (Certo et al., 2006; Brunelle et al., 2009; Goldstein et al., 2005; Waterhouse et al., 2006). Furthermore, we reported that loss of BAX and BAK, required for inducing MOMP, abrogated the effects of venetoclax on ETC metabolism (Guieze et al., 2019). Hence, we prefer describing venetoclax as a BCL-2 "antagonist" rather than "inhibitor" because "inhibitor" implies that an enzymatic function is being modulated. Instead, BH3 mimetics like venetoclax bind at a very specific site on BCL-2 to displace pro-apoptotic proteins from that binding site. There is no evidence that this site bears any enzymatic activity that could be inhibited by a BH3 mimetic.

While mitochondrial apoptotic priming was consistently reduced when BH3 mimetic resistance was acquired, DBP could nonetheless identify persistent drug vulnerabilities in the resistant models. Note that it was not the case that novel vulnerabilities absent in the parental clone were identified. Instead, DBP showed that, while apoptotic signaling induction was reduced for nearly all drugs in BH3-mimetic-resistant models, for a few drugs apoptotic signaling and *in vivo* activity persisted in the resistant model, including FLT3 inhibitors and SMAC mimetics. These results not only suggested combination strategies to be exploited (venetoclax and FLT3 inhibition is already being tested in the clinic), but also a general and personalized strategy for deploying combinations in the setting of BH3 mimetic resistance.

We also demonstrated *in vivo* that the principle of myeloblasts resistant to venetoclax being sensitive to MCL-1 antagonism was reciprocal—myeloblasts resistant to MCL-1 antagonism were in turn sensitive to BCL-2 antagonism. It is important to note, however, that while it might be clinically desirable that this would be an *enhanced* sensitivity to the complementary BH3 mimetic, it was more a *persistent* sensitivity. For MCL-1 and FLT3 inhibition it appears that two competing effects are at work in venetoclax resistance clones. There is a simultaneous observation showing increasing sensitivity (e.g., increased MCL:BIM complexes or enhanced FLT3 pathway signaling) but at the same time there is reduced MOM sensitivity to apoptotic signaling (perhaps due to reduced BAK expression). The result of these competing effects is roughly similar sensitivity in parental and venetoclax-resistant myeloblasts.

Although studies have reported synergy between BCL-2 and MCL-1 antagonists, much of the evidence on combination efficacy was derived from the activity of these drugs in non-resistant settings (Caenepeel et al., 2018). Several exciting clinical trials (NCT03672695) are either open or soon to be open that will be studying the tolerability of such combination regimen. Our *in vivo* experiments provided some practical principles that might guide the construction of BH3 mimetic combination regimens in the clinic. First, continuous high-dose combinations may cause tumor lysis and intrinsic toxicity to normal cells. Second, while alternating schedules or reducing doses both reduce toxicity, reducing dosing but maintaining simultaneous exposure to BCL-2 and MCL-1 antagonism offers clearly better efficacy. Therefore, we would suggest that, as combinations of BH3 mimetics are utilized, creative scheduling rather than mandatory daily dosing should be explored to reduce toxicity, but that this should be done so that the two drugs are given on the same day, when possible, to maintain efficacy.

STAR★METHODS

Detailed methods are provided in the online version of this paper and include the following:

- KEY RESOURCES TABLE
- RESOURCE AVAILABILITY
  - Lead Contact
  - Materials Availability
  - Data and Code Availability
- EXPERIMENTAL MODEL AND SUBJECT DETAILS
  - Cell Lines and Culture Conditions
  - Mice and Housing Conditions
  - Human Subjects
- METHOD DETAILS
  - PDX Studies and Drug Administration In Vivo
  - Venetoclax-Resistant Cell Generation and Cell Viability Assays
  - BH3 Profiling

(C) Comparison of baseline mitochondrial priming of parental (P) and S63845-resistant (R) PDXs, determined by BH3 profiling (n = 3 mice/group).
(D) Heatmap of delta priming responses in the myeloblasts derived from parental and S63845-resistant PDXs at 16 h drug treatment, determined via DBP. Each entry reflects three independent mice as biological replicates of two technical replicates each.
(E and F) S63845-resistant myeloblasts from DFAM-61786 were transplanted into NSG mice and assigned to treatment arms. (E) Percentage of $hCD45^+$ peripheral blast reduction in response to venetoclax (100 mg/kg, p.o., 5 days/week), S63845 (25 mg/kg, i.v., 2 days/week), and combination treatment. Mean ± SD, n = 5 mice; ***$p < 0.001$; one-way ANOVA. (F) Corresponding Kaplan-Meier survival curve. *$p < 0.05$, **$p < 0.01$; log rank test.
(G) Percentage of $hCD45^+$ peripheral blast reduction and corresponding Kaplan-Meier survival curve in response to quizartinib (10 mg/kg, i.p., 5 days/week). Mean ± SD, n = 5 mice.
(H) Percentage of $hCD45^+$ blast reduction across different compartments. Mean ± SD, n = 5 mice; *$p < 0.05$, **$p < 0.05$; two-tailed Student's t test.
See also Figure S8.

- Dynamic BH3 Profiling (DBP)
- Immunoblotting Assay
- Co-immunoprecipitation Assay
- Digital Droplet PCR
- RNA-seq
- Rapid Heme Panel Assay
- Quantitative PCR for BCL-2 Family Proteins

● QUANTIFICATION AND STATISTICAL ANALYSIS

SUPPLEMENTAL INFORMATION

Supplemental Information can be found online at https://doi.org/10.1016/j.ccell.2020.10.010.

ACKNOWLEDGMENTS

We thank Marie Schoumacher and Sébastien Banquet from Servier oncology R&D unit for providing S63845 and for critical review of the manuscript. S.B. is a recipient of a Career Development Award from the LLS, Basic Cancer Research Fellowship award from AACR, and Claudia-Adams Barr Award from DFCI. J.S.G. is a recipient of a Career Development Award from Conquer Cancer Foundation, and a Translational Research Project Award from the LLS. A.L. acknowledges support from P01 CA066996 and Ludwig Center at Harvard.

AUTHORS CONTRIBUTIONS

S.B. and A.L. conceptualized study, designed the experiments, analyzed data, and wrote the manuscript. J.S.G. designed the experiments, provided the patient samples, and analyzed the data. D.M.W. designed the experiments and provided PDX models. M.S.P., E.A.O., B.Y., S.A., J.A.R., T.M., H.Z., Y.K., A.M., A.J.L., S.R.B., A.K.M., and S.S. designed and performed the experiments, and analyzed the data. B.L. performed RNA sequencing computational analysis. Y.W., E.M., E.H., and C.P.P. analyzed the data.

DECLARATION OF INTERESTS

A.L. has consulted for and has received research support from AbbVie, Novartis, and AstraZeneca. He serves on the scientific advisory board of Flash Therapeutics, Dialectic Therapeutics, and Zentalis. J.S.G. received research funding from AbbVie, Genentech, Lilly, and Pfizer. She served on AbbVie advisory board. D.M.W. received research support from Novartis, Abbvie, AstraZeneca, Aileron, Daiichi-Sankyo, and Verastem. He is a founder and equity holder of Ajax Therapeutics and Travera. He serves on scientific advisory boards of Bantam Therapeutics, EDO Mundipharma, and Ajax Therapeutics.

Received: January 3, 2020
Revised: August 4, 2020
Accepted: October 7, 2020
Published: October 29, 2020

REFERENCES

Blombery, P., Anderson, M.A., Gong, J.N., Thijssen, R., Birkinshaw, R.W., Thompson, E.R., Teh, C.E., Nguyen, T., Xu, Z., Flensburg, C., et al. (2019). Acquisition of the recurrent Gly101Val mutation in BCL2 confers resistance to venetoclax in patients with progressive chronic lymphocytic leukemia. Cancer Discov. *9*, 342–353.

Brunelle, J.K., Ryan, J., Yecies, D., Opferman, J.T., and Letai, A. (2009). MCL-1-dependent leukemia cells are more sensitive to chemotherapy than BCL-2-dependent counterparts. J. Cell Biol. *187*, 429–442.

Caenepeel, S., Brown, S.P., Belmontes, B., Moody, G., Keegan, K.S., Chui, D., Whittington, D.A., Huang, X., Poppe, L., Cheng, A.C., et al. (2018). AMG 176, a selective MCL1 inhibitor, is effective in hematologic cancer models alone and in combination with established therapies. Cancer Discov. *8*, 1582–1597.

Certo, M., del Gaizo Moore, V., Nishino, M., Wei, G., Korsmeyer, S., Armstrong, S.A., and Letai, A. (2006). Mitochondria primed by death signals determine cellular addiction to antiapoptotic BCL-2 family members. Cancer Cell *9*, 351–365.

Chen, X., Glytsou, C., Zhou, H., Narang, S., Reyna, D.E., Lopez, A., Sakellaropoulos, T., Gong, Y., Kloetgen, A., Yap, Y.S., et al. (2019). Targeting mitochondrial structure sensitizes acute myeloid leukemia to venetoclax treatment. Cancer Discov. *9*, 890–909.

Chonghaile, T.N., Roderick, J.E., Glenfield, C., Ryan, J., Sallan, S.E., Silverman, L.B., Loh, M.L., Hunger, S.P., Wood, B., Deangelo, D.J., et al. (2014). Maturation stage of T-cell acute lymphoblastic leukemia determines BCL-2 versus BCL-XL dependence and sensitivity to ABT-199. Cancer Discov. *4*, 1074–1087.

Cidado, J., Boiko, S., Proia, T., Ferguson, D., Criscione, S.W., San Martin, M., Pop-Damkov, P., Su, N., Roamio Franklin, V.N., Sekhar Reddy Chilamakuri, C., et al. (2020). AZD4573 is a highly selective CDK9 inhibitor that suppresses Mcl-1 and induces apoptosis in hematological cancer cells. Clin. Cancer Res. *26*, 922–934.

Condon, S.M., Mitsuuchi, Y., Deng, Y., Laporte, M.G., Rippin, S.R., Haimowitz, T., Alexander, M.D., Kumar, P.T., Hendi, M.S., Lee, Y.H., et al. (2014). Birinapant, a smac-mimetic with improved tolerability for the treatment of solid tumors and hematological malignancies. J. Med. Chem. *57*, 3666–3677.

Dai, H., Ding, H., Meng, X.W., Lee, S.H., Schneider, P.A., and Kaufmann, S.H. (2013). Contribution of Bcl-2 phosphorylation to Bak binding and drug resistance. Cancer Res. *73*, 6998–7008.

Del Gaizo Moore, V., Brown, J.R., Certo, M., Love, T.M., Novina, C.D., and Letai, A. (2007). Chronic lymphocytic leukemia requires BCL2 to sequester prodeath BIM, explaining sensitivity to BCL2 antagonist ABT-737. J. Clin. Invest. *117*, 112–121.

Del Gaizo Moore, V., Schlis, K.D., Sallan, S.E., Armstrong, S.A., and Letai, A. (2008). BCL-2 dependence and ABT-737 sensitivity in acute lymphoblastic leukemia. Blood *111*, 2300–2309.

Deng, J., Carlson, N., Takeyama, K., Dal Cin, P., Shipp, M., and Letai, A. (2007). BH3 profiling identifies three distinct classes of apoptotic blocks to predict response to ABT-737 and conventional chemotherapeutic agents. Cancer Cell *12*, 171–185.

Di Veroli, G.Y., Fornari, C., Wang, D., Mollard, S., Bramhall, J.L., Richards, F.M., and Jodrell, D.I. (2016). Combenefit: an interactive platform for the analysis and visualization of drug combinations. Bioinformatics *32*, 2866–2868.

DiNardo, C.D., Pratz, K., Pullarkat, V., Jonas, B.A., Arellano, M., Becker, P.S., Frankfurt, O., Konopleva, M., Wei, A.H., Kantarjian, H.M., et al. (2019). Venetoclax combined with decitabine or azacitidine in treatment-naive, elderly patients with acute myeloid leukemia. Blood *133*, 7–17.

DiNardo, C.D., Tiong, I.S., Quaglieri, A., Macraild, S., Loghavi, S., Brown, F.C., Thijssen, R., Pomilio, G., Ivey, A., Salmon, J.M., et al. (2020). Molecular patterns of response and treatment failure after frontline venetoclax combinations in older patients with AML. Blood *135*, 791–803.

Dobin, A., Davis, C.A., Schlesinger, F., Drenkow, J., Zaleski, C., Jha, S., Batut, P., Chaisson, M., and Gingeras, T.R. (2013). STAR: ultrafast universal RNA-seq aligner. Bioinformatics *29*, 15–21.

Goldstein, J.C., Munoz-Pinedo, C., Ricci, J.E., Adams, S.R., Kelekar, A., Schuler, M., Tsien, R.Y., and Green, D.R. (2005). Cytochrome c is released in a single step during apoptosis. Cell Death Differ. *12*, 453–462.

Guieze, R., Liu, V.M., Rosebrock, D., Jourdain, A.A., Hernandez-Sanchez, M., Martinez Zurita, A., Sun, J., Ten Hacken, E., Baranowski, K., Thompson, P.A., et al. (2019). Mitochondrial reprogramming underlies resistance to BCL-2 inhibition in lymphoid malignancies. Cancer Cell *36*, 369–384 e13.

Kale, J., Kutuk, O., Brito, G.C., Andrews, T.S., Leber, B., Letai, A., and Andrews, D.W. (2018). Phosphorylation switches Bax from promoting to inhibiting apoptosis thereby increasing drug resistance. EMBO Rep. *19*, e45235.

Khan, S., Zhang, X., Lv, D., Zhang, Q., He, Y., Zhang, P., Liu, X., Thummuri, D., Yuan, Y., Wiegand, J.S., et al. (2019). A selective BCL-XL PROTAC degrader achieves safe and potent antitumor activity. Nat. Med. *25*, 1938–1947.

Kluin, R.J.C., Kemper, K., Kuilman, T., De Ruiter, J.R., Iyer, V., Forment, J.V., Cornelissen-Steijger, P., De Rink, I., Ter Brugge, P., Song, J.Y., et al. (2018). XenofilteR: computational deconvolution of mouse and human reads in tumor xenograft sequence data. BMC Bioinformatics *19*, 366.

Kluk, M.J., Lindsley, R.C., Aster, J.C., Lindeman, N.I., Szeto, D., Hall, D., and Kuo, F.C. (2016). Validation and implementation of a custom next-generation sequencing clinical assay for hematologic malignancies. J. Mol. Diagn. *18*, 507–515.

Konopleva, M., and Letai, A. (2018). BCL-2 inhibition in AML: an unexpected bonus? Blood *132*, 1007–1012.

Konopleva, M., Pollyea, D.A., Potluri, J., Chyla, B., Hogdal, L., Busman, T., McKeegan, E., Salem, A.H., Zhu, M., Ricker, J.L., et al. (2016). Efficacy and biological correlates of response in a phase II study of venetoclax monotherapy in patients with acute myelogenous leukemia. Cancer Discov. *6*, 1106–1117.

Kotschy, A., Szlavik, Z., Murray, J., Davidson, J., Maragno, A.L., Le Toumelin-Braizat, G., Chanrion, M., Kelly, G.L., Gong, J.N., Moujalled, D.M., et al. (2016). The MCL1 inhibitor S63845 is tolerable and effective in diverse cancer models. Nature *538*, 477–482.

Matulis, S.M., Gupta, V.A., Nooka, A.K., Hollen, H.V., Kaufman, J.L., Lonial, S., and Boise, L.H. (2016). Dexamethasone treatment promotes Bcl-2 dependence in multiple myeloma resulting in sensitivity to venetoclax. Leukemia *30*, 1086–1093.

Montero, J., Sarosiek, K.A., Deangelo, J.D., Maertens, O., Ryan, J., Ercan, D., Piao, H., Horowitz, N.S., Berkowitz, R.S., Matulonis, U., et al. (2015). Drug-induced death signaling strategy rapidly predicts cancer response to chemotherapy. Cell *160*, 977–989.

Montero, J., Stephansky, J., Cai, T., Griffin, G.K., Cabal-Hierro, L., Togami, K., Hogdal, L.J., Galinsky, I., Morgan, E.A., Aster, J.C., et al. (2017). Blastic plasmacytoid dendritic cell neoplasm is dependent on BCL2 and sensitive to venetoclax. Cancer Discov. *7*, 156–164.

Morales, A.A., Kurtoglu, M., Matulis, S.M., Liu, J., Siefker, D., Gutman, D.M., Kaufman, J.L., Lee, K.P., Lonial, S., and Boise, L.H. (2011). Distribution of Bim determines Mcl-1 dependence or codependence with Bcl-xL/Bcl-2 in Mcl-1-expressing myeloma cells. Blood *118*, 1329–1339.

Nangia, V., Siddiqui, F.M., Caenepeel, S., Timonina, D., Bilton, S.J., Phan, N., Gomez-Caraballo, M., Archibald, H.L., Li, C., Fraser, C., et al. (2018). Exploiting MCL1 dependency with combination MEK + MCL1 inhibitors leads to induction of apoptosis and tumor regression in KRAS-mutant non-small cell lung cancer. Cancer Discov. *8*, 1598–1613.

Nechiporuk, T., Kurtz, S.E., Nikolova, O., Liu, T., Jones, C.L., D'Alessandro, A., Culp-Hill, R., D'Almeida, A., Joshi, S.K., Rosenberg, M., et al. (2019). The TP53 apoptotic network is a primary mediator of resistance to BCL2 inhibition in AML cells. Cancer Discov. *9*, 910–925.

Pan, R., Hogdal, L.J., Benito, J.M., Bucci, D., Han, L., Borthakur, G., Cortes, J., Deangelo, D.J., Debose, L., Mu, H., et al. (2014). Selective BCL-2 inhibition by ABT-199 causes on-target cell death in acute myeloid leukemia. Cancer Discov. *4*, 362–375.

Patro, R., Duggal, G., Love, M.I., Irizarry, R.A., and Kingsford, C. (2017). Salmon provides fast and bias-aware quantification of transcript expression. Nat. Methods *14*, 417–419.

Pollyea, D.A., Stevens, B.M., Jones, C.L., Winters, A., Pei, S., Minhajuddin, M., D'Alessandro, A., Culp-Hill, R., Riemondy, K.A., Gillen, A.E., et al. (2018). Venetoclax with azacitidine disrupts energy metabolism and targets leukemia stem cells in patients with acute myeloid leukemia. Nat. Med. *24*, 1859–1866.

Ramsey, H.E., Fischer, M.A., Lee, T., Gorska, A.E., Arrate, M.P., Fuller, L., Boyd, K.L., Strickland, S.A., Sensintaffar, J., Hogdal, L.J., et al. (2018). A novel MCL1 inhibitor combined with venetoclax rescues venetoclax-resistant acute myelogenous leukemia. Cancer Discov. *8*, 1566–1581.

Ricci, J.E., Waterhouse, N., and Green, D.R. (2003). Mitochondrial functions during cell death, a complex (I-V) dilemma. Cell Death Differ. *10*, 488–492.

Ritchie, M.E., Phipson, B., Wu, D., Hu, Y., Law, C.W., Shi, W., and Smyth, G.K. (2015). Limma powers differential expression analyses for RNA-sequencing and microarray studies. Nucleic Acids Res. *43*, e47.

Roberts, A.W., Davids, M.S., Pagel, J.M., Kahl, B.S., Puvvada, S.D., Gerecitano, J.F., Kipps, T.J., Anderson, M.A., Brown, J.R., Gressick, L., et al. (2016). Targeting BCL2 with venetoclax in relapsed chronic lymphocytic leukemia. N. Engl. J. Med. *374*, 311–322.

Roca-Portoles, A., Rodriguez-Blanco, G., Sumpton, D., Cloix, C., Mullin, M., Mackay, G.M., O'Neill, K., Lemgruber, L., Luo, X., and Tait, S.W.G. (2020). Venetoclax causes metabolic reprogramming independent of BCL-2 inhibition. Cell Death Dis. *11*, 616.

Ryan, J., Montero, J., Rocco, J., and Letai, A. (2016). iBH3: simple, fixable BH3 profiling to determine apoptotic priming in primary tissue by flow cytometry. Biol. Chem. *397*, 671–678.

Sarosiek, K.A., Chi, X., Bachman, J.A., Sims, J.J., Montero, J., Patel, L., Flanagan, A., Andrews, D.W., Sorger, P., and Letai, A. (2013). BID preferentially activates BAK while BIM preferentially activates BAX, affecting chemotherapy response. Mol. Cell *51*, 751–765.

Schneider, C.A., Rasband, W.S., and Eliceiri, K.W. (2012). NIH Image to ImageJ: 25 years of image analysis. Nat. Methods *9*, 671–675.

Sharon, D., Cathelin, S., Mirali, S., Di Trani, J.M., Yanofsky, D.J., Keon, K.A., Rubinstein, J.L., Schimmer, A.D., Ketela, T., and Chan, S.M. (2019). Inhibition of mitochondrial translation overcomes venetoclax resistance in AML through activation of the integrated stress response. Sci. Transl. Med. *11*, eaax2863.

Soneson, C., Love, M.I., and Robinson, M.D. (2015). Differential analyses for RNA-seq: transcript-level estimates improve gene-level inferences. F1000Res. *4*, 1521.

Souers, A.J., Leverson, J.D., Boghaert, E.R., Ackler, S.L., Catron, N.D., Chen, J., Dayton, B.D., Ding, H., Enschede, S.H., Fairbrother, W.J., et al. (2013). ABT-199, a potent and selective BCL-2 inhibitor, achieves antitumor activity while sparing platelets. Nat. Med. *19*, 202–208.

Takahashi, S. (2011). Downstream molecular pathways of FLT3 in the pathogenesis of acute myeloid leukemia: biology and therapeutic implications. J. Hematol. Oncol. *4*, 13.

Tausch, E., Close, W., Dolnik, A., Bloehdorn, J., Chyla, B., Bullinger, L., Dohner, H., Mertens, D., and Stilgenbauer, S. (2019). Venetoclax resistance and acquired BCL2 mutations in chronic lymphocytic leukemia. Haematologica *104*, e434–e437.

Townsend, E.C., Murakami, M.A., Christodoulou, A., Christie, A.L., Koster, J., Desouza, T.A., Morgan, E.A., Kallgren, S.P., Liu, H., Wu, S.C., et al. (2016). The public repository of xenografts enables discovery and randomized phase II-like trials in mice. Cancer Cell *29*, 574–586.

Tron, A.E., Belmonte, M.A., Adam, A., Aquila, B.M., Boise, L.H., Chiarparin, E., Cidado, J., Embrey, K.J., Gangl, E., Gibbons, F.D., et al. (2018). Discovery of Mcl-1-specific inhibitor AZD5991 and preclinical activity in multiple myeloma and acute myeloid leukemia. Nat. Commun. *9*, 5341.

Vo, T.T., Ryan, J., Carrasco, R., Neuberg, D., Rossi, D.J., Stone, R.M., Deangelo, D.J., Frattini, M.G., and Letai, A. (2012). Relative mitochondrial priming of myeloblasts and normal HSCs determines chemotherapeutic success in AML. Cell *151*, 344–355.

Wang, X., Bathina, M., Lynch, J., Koss, B., Calabrese, C., Frase, S., Schuetz, J.D., Rehg, J.E., and Opferman, J.T. (2013). Deletion of MCL-1 causes lethal cardiac failure and mitochondrial dysfunction. Genes Dev. *27*, 1351–1364.

Waterhouse, N.J., Goldstein, J.C., von Ahsen, O., Schuler, M., Newmeyer, D.D., and Green, D.R. (2001). Cytochrome c maintains mitochondrial transmembrane potential and ATP generation after outer mitochondrial membrane permeabilization during the apoptotic process. J. Cell Biol. *153*, 319–328.

Waterhouse, N.J., Sedelies, K.A., Sutton, V.R., Pinkoski, M.J., Thia, K.Y., Johnstone, R., Bird, P.I., Green, D.R., and Trapani, J.A. (2006). Functional dissociation of DeltaPsim and cytochrome c release defines the contribution

of mitochondria upstream of caspase activation during granzyme B-induced apoptosis. Cell Death Differ. *13*, 607–618.

Wei, A.H., Montesinos, P., Ivanov, V., Dinardo, C.D., Novak, J., Laribi, K., Kim, I., Stevens, D., Fiedler, W., Pagoni, M., et al. (2020). Venetoclax plus LDAC for patients with untreated AML ineligible for intensive chemotherapy: phase 3 randomized placebo-controlled trial. Blood *135*, 2137–2145.

Wei, A.H., Strickland, S.A., Jr., Hou, J.Z., Fiedler, W., Lin, T.L., Walter, R.B., Enjeti, A., Tiong, I.S., Savona, M., Lee, S., et al. (2019). Venetoclax combined with low-dose cytarabine for previously untreated patients with acute myeloid leukemia: results from a phase Ib/II study. J. Clin. Oncol. *37*, 1277–1284.

Yecies, D., Carlson, N.E., Deng, J., and Letai, A. (2010). Acquired resistance to ABT-737 in lymphoma cells that up-regulate MCL-1 and BFL-1. Blood *115*, 3304–3313.

Yu, G., Wang, L.G., Han, Y., and He, Q.Y. (2012). clusterProfiler: an R package for comparing biological themes among gene clusters. OMICS *16*, 284–287.

Zarrinkar, P.P., Gunawardane, R.N., Cramer, M.D., Gardner, M.F., Brigham, D., Belli, B., Karaman, M.W., Pratz, K.W., Pallares, G., Chao, Q., et al. (2009). AC220 is a uniquely potent and selective inhibitor of FLT3 for the treatment of acute myeloid leukemia (AML). Blood *114*, 2984–2992.

STAR★METHODS

KEY RESOURCES TABLE

REAGENT or RESOURCE	SOURCE	IDENTIFIER
Antibodies		
Mouse anti-human CD45 HI30 BV421	BD Biosciences	Cat# 563879; RRID: AB_2744402
Mouse anti-human CD33 WM53 PE	BD Biosciences	Cat# 555450; RRID: AB_395843
Zombie Yellow Fixable Viability Kit	BioLegend	Cat# 423104
Human FcR block	Miltenyi Biotec	Cat# 130-059-901
Mouse anti-human Cytochrome c FITC 6H2.B4	Biolegend	Cat# 983502; RRID: AB_2749869
Mouse anti-human Cytochrome c Alexafluor 647 6H2.B4	Biolegend	Cat# 612310; RRID: AB_2565241
Rabbit polyclonal AKT	Cell Signaling	Cat# 9272; RRID: AB_329827
Rabbit mBAD D24A9	Cell Signaling	Cat# 9239; RRID: AB_2062172
Rabbit mBAK D4E4	Cell Signaling	Cat# 12105; RRID: AB_271685
Rabbit polyclonal BAX	Cell Signaling	Cat# 2772; RRID: AB_10695870
BCL-2 (124) Mouse mAb	Cell Signaling	Cat# 15071; RRID: AB_2744528
Rabbit mAb BCL-XL 54H6	Cell Signaling	Cat# 2764; RRID: AB_2228008
Rabbit mAb BIM C34C5	Cell Signaling	Cat# 2933; RRID: AB_1030947
Rabbit polyclonal CLPB	Abcam	Cat# 87253; RRID: AB_1952530
Rabbit polyclonal p44/42 MAPK (Erk 1/2)	Cell Signaling	Cat# 9102; RRID: AB_330744
Rabbit mFLT3 8F2	Cell Signaling	Cat# 3462; RRID: AB_2107052
Rabbit mAb MCL-1 D35A5	Cell Signaling	Cat# 5453; RRID: AB_10694494
Rabbit mAb MCL-1 D2W9E	Cell Signaling	Cat# 94296; RRID: AB_2722740
Polyclonal Normal Rabbit IgG	Cell Signaling	Cat# 2729
Rabbit mAb NOXA D8L7U	Cell Signaling	Cat# 14766; RRID: AB_2798602
Rabbit polyclonal p-AKT Ser 473	Cell Signaling	Cat# 9271; RRID: AB_329825
Rabbit polyclonal p-BAX Ser 184	ThermoFisher	Cat# PA5-39778; RRID: AB_2556329
Rabbit mAb phospho-BCL-2 Ser 70 5H2	Cell Signaling	Cat# 2827; RRID: AB_659950
Rabbit mAb phospho-FLT3 Tyr 842 10A8	Cell Signaling	Cat# 4577; RRID: AB_916078
Rabbit polyclonal p-p44/42 MAPK (Erk1/2) Thr 202/Tyr 204	Cell Signaling	Cat# 9101; RRID: AB_331646
Rabbit mAb phospho-STAT-5 Tyr 694 C11C5	Cell Signaling	Cat# 9359; RRID: AB_823649
Rabbit polyclonal P53	Cell Signaling	Cat# 9282; RRID: AB_331476
Rabbit mAb STAT-5 D3N2B	Cell Signaling	Cat# 25656; RRID: AB_2798908
Rabbit mAb Vinculin E1E9V XP	Cell Signaling	Cat# 13901; RRID: AB_2728768
Anti-rabbit IgG HRP-linked antibody	Cell Signaling	Cat# 7074; RRID: AB_2099233
Anti-mouse IgG for IP (HRP)	Abcam	Cat# 131368
VeriBlot for IP Detection Reagent (HRP)	Abcam	Cat# 131366
Biological Samples		
Patient Derived Xenograft models	PRoXe or cBioportal	https://proxe.shinyapps.io/PRoXe/
AML primary tumors	This paper	As indicated in the paper
Chemicals, Peptides, and Recombinant Proteins		
RBC Lysis Solution	Qiagen	Cat# 158904
Venetoclax	Medchem Express	Cat# HY-15531
Phosal 50 PG	Fisher Scientific	Cat# NC0130871
PEG 400	Sigma Aldrich	Cat# 202398-500G
Quizartinib	Selleckchem	Cat# S1526
Hydroxypropyl-β-cyclodextrin powder	Sigma Aldrich	Cat# C0926-5G

(*Continued on next page*)

Continued

REAGENT or RESOURCE	SOURCE	IDENTIFIER
S63845	Servier/Novartis	Provided
D-α-Tocopherol polyethylene glycol 1000 succinate	Sigma Aldrich	Cat# 57668
LCL-161	Supplied by Novartis	Kindly Provided
Birinapant	TargetMol Inc.	Cat# T6007
NVP-MIK665	Supplied by Novartis	Provided
Ficoll	Fisher Scientific	Cat# 45001749
Alamethicin	Enzo	Cat# BML-A150-0005
Digitonin	Sigma-Aldrich	Cat# D5628
RIPA buffer	Sigma-Aldrich	Cat# R0278-50ML
NP-40	Fisher Scientific	NC9983875
cOmplete Mini EDTA-free Protease inhibitor cocktail	Millipore Sigma	Cat# 11836170001
PhosSTOP Phosphatase inhibitor	Sigma Aldrich	Cat# 4906837001
360 GC enhancer	Applied Biosytsems	Cat# 4398848
hBIM Acetyl-MRPEIWIAQELRRIGDEFNA-Amide	New England Peptide	Custom
hBID-Y Acetyl -EDIIRNIARHLAQVGDSMDRY- Amide	New England Peptide	Custom
mBAD Acetyl -LWAAQRYGRELRRMSDEFEGSFKGL-Amide	New England Peptide	Custom
mNOXA Acetyl -AELPPEFAAQLRKIGDKVYC- Amide	New England Peptide	Custom
Puma Acetyl -EQWAREIGAQLRRMADDLNA- Amide	New England Peptide	Custom
Hrk-Y Acetyl -SSAAQLTAARLKALGDELHQY- Amide	New England Peptide	Custom
MS1 Acetyl-RPEIWMTQGLRRLGDEINAYYAR-Amide	New England Peptide	Custom
FS1 Acetyl-QWVREIAAGLRLAADNVNAQLER-Amide	New England Peptide	Custom
JQ-1	Jun Qi Lab	Kindly provided
OTXO-15	Jun Qi Lab	Kindly provided
TEN-010	Jun Qi Lab	Kindly provided
GSK2830371	Ben Ebert Lab	Kindly provided
MSK777	Mark Frattini Lab	Kindly provided
Quizartinib (AC220)	Selleckchem	Cat# S1526
TAE684	Selleckchem	Cat# S1108
Etoposide	Selleckchem	Cat# S1225
Daunorubicin	Selleckchem	Cat# S3035
Cytarabine	Selleckchem	Cat# S1648
AZD 5991	Selleckchem	Cat# S8643
AZD 4573	Selleckchem	Cat# S8719
Parthenolide	Selleckchem	Cat# S2341
KPT-330	Selleckchem	Cat# S7252
P22077	Selleckchem	Cat# S7133
Lenalidomide	Selleckchem	Cat# S1029
JIB04	Selleckchem	Cat# S7281
Panabinostat	Selleckchem	Cat# S1030
Azacytidine	Selleckchem	Cat# S1782
Volasertib	Selleckchem	Cat# S2235
AZD 2014	Selleckchem	Cat# S2783
BEZ235	Selleckchem	Cat# S1009
Selumetinib	Selleckchem	Cat# S1008
Erlotinib	Selleckchem	Cat# S7786
Vemurafenib	Selleckchem	Cat# S1267
Ruxolitinib	Selleckchem	Cat# S1378
Dasatinib	Selleckchem	Cat# S1021

(*Continued on next page*)

Continued

REAGENT or RESOURCE	SOURCE	IDENTIFIER
Imatinib	Selleckchem	Cat# S2475
MK2206	Selleckchem	Cat# S1078
Trametinib	Selleckchem	Cat# S2673
Cobimetinib	Selleckchem	Cat# S8041
Sorafenib	Selleckchem	Cat# S7397
Crenolanib	Selleckchem	Cat# S2730
Gilteritinib	Selleckchem	Cat# S7754
Critical Commercial Assays		
MycoAlert mycoplasma detection kit	Lonza	Cat# LT07-318
CellTiter-Glo	Promega	Cat# G7572
Dynabeads protein G immunoprecipitation kit	ThermoFisher	Cat# 10007D
mRNA Isolation Kit	Miltenyi Biotec	Cat# 130-092-520
True-SeqRNA Sample Prep Kit	Illumina	Cat# RS-122-2001
DNA mini kit	Qiagen	Cat# 51304
RNeasy mini kit	Qiagen	Cat# 74104
High-capacity cDNA Reverse Transcription Kit	Applied Biosystems	Cat# 4368814
Taqman Fast Advanced Master Mix	Life Technologies	Cat# 4444557
Deposited Data		
RNAseq data	NCBI sequence read archive (SRA)	SRA: PRJNA664736
Nextgen sequencing data (RHP)	NCBI sequence read archive (SRA)	SRA: PRJNA664736
Original uncropped raw gel images	Mendeley	Mendeley: http://dx.doi.org/10.17632/ydxbsjg948.1
Experimental Models: Cell Lines		
Molm-13	DMSZ	ACC 554
Molm-14	DMSZ	ACC 777
OCI-AML-2	DMSZ	ACC 99
OCI-AML-3	DMSZ	ACC 582
THP-1	ATCC	TIB-202
M-V-411	ATCC	CRL-9591
HL-60	ATCC	CCL-240
KG-1	ATCC	CCL-246
Experimental Models: Organisms/Strains		
Mouse model: NOD-scid IL2Rgammanull female mice	The Jackson Laboratory	005557
Oligonucleotides		
See Table S3		
Software and Algorithms		
STAR	(Dobin et al., 2013)	https://github.com/alexdobin/STAR
Xenofilter	(Kluin et al., 2018)	https://github.com/PeeperLab/XenofilteR
Salmon	(Patro et al., 2017)	https://github.com/COMBINE-lab/Salmon
Tximport (R package)	(Soneson et al., 2015)	https://github.com/mikelove/tximport
Limma	(Ritchie et al., 2015)	https://bioconductor.org/packages/release/bioc/html/limma.html
clusterProfiler	(Yu et al., 2012)	https://github.com/YuLab-SMU/clusterProfiler
Xenofilter	(Kluin et al., 2018)	https://github.com/PeeperLab/XenofilteR
Combenefit	(Di Veroli et al., 2016)	https://www.cruk.cam.ac.uk/research-groups/jodrell-group/combenefit
Prism 8	GraphPad	https://www.graphpad.com/
Biorender	Biorender.com	https://biorender.com/
Image J	Schneider et al., 2012	https://imagej.nih.gov/ij/

RESOURCE AVAILABILITY

Lead Contact

Further information and requests for resources and reagents should be directed to and will be fulfilled by the Lead Contact, Anthony Letai (Anthony_letai@dfci.harvard.edu).

Materials Availability

PDX models generated in this study have been deposited to the Public Repository of Xenografts (PRoXe). Requests can be made at https://proxe.shinyapps.io/PRoXe/

Data and Code Availability

The accession number for the RNAseq data and targeted exome sequencing data reported in this paper is NCBI Sequence Read Archive (SRA): PRJNA664736. The bioinformatics codes supporting the study are deposited in github (https://github.com). Original uncropped gel images deposited to Mendely Data: http://dx.doi.org/10.17632/ydxbsjg948.1.

EXPERIMENTAL MODEL AND SUBJECT DETAILS

Cell Lines and Culture Conditions

All cell lines were validated by STR profiling and tested negative for mycoplasma (MycoAlert mycoplasma detection kit; Lonza, GA, USA). Cell were cultured in a humidified incubator at 37° and 5% CO2. AML cell lines MOLM-13, MOLM-14, OCI-AML-2, OCI-AML-3, THP-1, and M-V-411 (sourced from ATCC) were cultured with heat inactivated RPMI-1640 (Invitrogen) and 10% fetal bovine serum. HL-60 and KG-1 were cultured with Iscove modified Dulbecco medium (Invitrogen) and 10% fetal bovine serum and 1% penicillin/streptomycin (Invitrogen). Early passages (P5-P7) after purchase were cryopreserved and thawed for the experiments. Cells beyond passage 15 were not used.

Mice and Housing Conditions

Animal experiments were performed after approval from the Dana Farber Cancer Center Committee on Use and Care of Animals and were conducted as per NIH guidelines for animal welfare. All animal procedures were performed in accordance with approved Institutional Animal Care and Use Committee (IACUC) guidelines at Dana-Farber cancer institute animal facility (IACUC protocol#14-038). Animals were housed and cared according to standard guidelines with free access to water and food. All experiments were performed on 6-8 weeks old, female NOD-scid IL2Rgammanull female NSG mice (Jackson labs stock#005557). Animals were randomly assigned to experimental groups.

Human Subjects

AML patient characteristics and clinical response are described in detail in Table S2. All samples were obtained after informed patient consent under IRB approved Dana-Farber Cancer Institute collection protocols. All patients included in this study received venetoclax plus azacitidine or decitabine.

METHOD DETAILS

PDX Studies and Drug Administration In Vivo

AML PDX models DFAM-61786, DFAM-15354, DFAM-58159, DFAM-68555, DFAL-49600, DFAM-61345, and DFAM-16835 are available from the Public Repository of Xenografts (PRoXe) (Townsend et al., 2016). Clinical details are summarized in Table S1. 6-8-weeks old, female NSG mice (Jackson Labs) were injected with passage-2 $0.6x10^6$ human leukemia cells intravenously (i.v.). Mice were bled weekly, and treatment was initiated when circulating disease was >5% as assessed by flow cytometry staining for hCD45 (clone HI30, BD Biosciences) and hCD33 (clone WM53, BD Biosciences). All blood samples were lysed with ammonium chloride red-blood-cell buffer (Qiagen) prior to staining. Clinical grade venetoclax (Medchem express) was formulated in a mixture of 60% phosal 50 PG, 30% PEG 400, and 10% EtOH. Quizartinib (Selleckchem) was formulated in 22% hydroxypropyl-β-cyclodextrin, S63845 was kindly provided by Servier/Novartis and was formulated in 2% VitaminE/TPGS in 0.9% NaCl. LCL-161 was kindly provided by Novartis and was formulated in 30% of 0.1N HCl and 70% of 100mM sodium acetate buffer at pH 4.5. Birinapant (#T6007, TargetMol Inc.) was formulated in Citrate buffer pH 5.5.

Venetoclax-Resistant Cell Generation and Cell Viability Assays

To create Venetoclax-resistant MOLM-13 cell line, we cultured cells in media supplemented with increasing concentrations of Venetoclax upto to 1.3umol/L for more than 8 weeks and were declared as resistant when they were able to maintain greater than 98% viability in the presence of the inhibitor. On the day of the experiment, cells were divided in two tubes: tube 1 cells were washed in media alone (no Venetoclax) to simulate a washout condition and tube 2 cells were washed with media containing Venetoclax. Cells from both tubes were plated in a 384-well plate in their respective media – without Venetoclax and with Venetoclax. The next day, cells were treated with a dose-response of NVP-MIK665 (clinical analog of S63845) at concentrations ranging from 5.3 pmol/L to

25umol/L. Cells and compounds were allowed to incubate for 72hrs. Cell viability was measured using CellTiter-Glo reagent (Promega) according to the manufacturer's instructions. Absolute viability values were converted to percentage viability versus DMSO control treatment and then, nonlinear fit of Log (inhibitor) vs. response – Variable slope (four parameters) was performed in GraphPad Prism v8.0 to obtain the IC50 values.

BH3 Profiling

Pretreatment bone marrow aspirates or peripheral blood samples from patients were obtained, and mononuclear cells were isolated using a Ficoll-paque Plus (GE Health Care). Cells were stained with 1:100 live/dead fixable zombie yellow stain (BioLegend) in PBS for 15 minutes at room temperature, washed with PBS, and subsequently stained with 1:100 CD45-BV421 clone HI30 (BD Biosciences) and 1:100 CD33-PE clone WM53 (BD Biosciences) in FACS buffer (2% FBS in PBS) on ice for 30 minutes with 1:100 human FcR block (Miltenyi Biotec). BH3 profiling was performed as previously described(Ryan et al., 2016). Cells were exposed to increasing concentration of synthetic BH3 peptides in MEB buffer (150mM mannitol, 10mM HEPES-KOH pH 7.5, 50mM KCl, 0.02mM EGTA, 0.02mM EDTA, 0.1% BSA and 5mM Succinate) for 60 minutes after plasma membrane permeabilization with digitonin (0.002%). After 60 minutes peptide exposure at room temperature cells were fixed using 4% formaldehyde for 15 minutes, followed by neutralization for 10 minutes using N2 buffer (1.7M Tris, 1.25M Glycine pH 9.1). Sensitivity to BH3 peptides were measured as cytochrome *c* loss using anti-cytochrome c Alexafluor 647 antibody (Clone 6H2.B4, Biolegend) in staining buffer (10% BSA, 2% Tween20, PBS) via FACS by a gating strategy, in which a gate was drawn around the DMSO-negative control to depict 100% cytochrome *c* retention. DMSO was used as a negative control for cytochrome *c* retention, whereas alamethicin was used as a positive control for 100% cytochrome *c* release. Cytochrome *c* loss was calculated using the following equation: [Cytochrome *c* loss = 100 − (% of cells within cytochrome *c* retention gate)]. AML blasts were identified by CD45 lo-mid/SSC-low.

Dynamic BH3 Profiling (DBP)

Pre- and post- venetoclax resistant myeloblasts from PDXs were exposed to a panel of targeted agents for 16 hours or DMSO (control) followed by BH3 profiling using BIM peptides as described above(Montero et al., 2015). The read-out for drug-induced change in priming is defined as "delta priming" (calculation: delta priming = cytochrome *c* loss^{drug} - cytochrome *c* loss^{DMSO}). An acceptable delta priming threshold calculated by cytochrome *c* release caused by 3(mean ± SD) of DMSO treated wells was used to determine significance.

Immunoblotting Assay

Whole-cell extracts were prepared by lysing cells for 30 min on ice in RIPA lysis buffer (Sigma-Aldrich) supplemented with protease inhibitor (Millipore) and phosphatase inhibitor (Sigma-Aldrich). Cellular lysates were assayed for protein concentration using Coomassie Protein Assay Reagent (Pierce) in 96 well-plates using a Bio-Rad Benchmark Microplate Reader. Whole cell lysates were separated through SDS polyacrylamide gels (4–12%) and transferred to nitrocellulose membrane (Bio-Rad Laboratories, Inc.). Membranes were blocked with 5% milk powder in 0.1% Tween20 in 1x PBS (PBS-T) for 1 hr at room temperature followed by incubation with primary antibodies diluted in 2.5% milk PBS-T. ImmunoCruz Western Blotting Luminol Reagent (Santa Cruz Biotechnology, Inc.) was used to visualize protein levels with light sensitive-films (Phenix Research). Immunoblots were quantified using ImageJ software(Schneider et al., 2012). For image processing, scanned PDFs were aligned and cropped in Adobe photoshop, followed by brightness/contrast adjustment in PowerPoint. Final compilation was performed in Adobe illustrator. Raw uncropped images can be accessed on Mendeley: http://dx.doi.org/10.17632/ydxbsjg948.1.

Co-immunoprecipitation Assay

Viably frozen PDX cells pre- and post-venetoclax resistance were lysed in RIPA buffer (Sigma-Aldrich) for immunoblotting and NP-40 buffer (50mM Tris-HCl pH 8.0; 150mM NaCl; 1% NP-40) for co-immunoprecipitation, where both were supplemented with protease inhibitor cocktail and phosphatase inhibitor. Immunoprecipitation was performed in 500μl of lysates containing 3x10^6 cells using Dynabeads protein G immunoprecipitation kit (Thermofisher Scientific), by following the manufacturer's protocol. Eluted proteins were analyzed by immunoblotting as described above. Antibodies used included AKT (Cell Signaling; 9272), BAD (Cell Signaling; 9239), BAK (Cell Signaling; 12105), BAX (Cell Signaling; 2772), BCL-2 (Cell Signaling; 15071), BCL-2 (Cell Signaling; 4223), BCL-XL (Cell Signaling; 2764), BIM (Cell Signaling; 2933), CLPB (Abcam; 87253), ERK (Cell Signaling; 9102), FLT3FLT3 (Cell Signaling; 3462), MCL-1 (Cell Signaling; 5453), MCL-1 (Cell Signaling; 94296), Normal Rabbit IgG (Cell Signaling; 2729), NOXA (Cell Signaling; 14766), p-AKT (Cell Signaling; 9271), p-BAX (ThermoFisher; PA5-39778), p-BCL-2 (Cell Signaling; 2827), p-FLT3 (Cell Signaling; 4577), P-p44/42 MAPK (Erk1/2) (Cell Signaling; 9101), p-STAT-5 (Cell Signaling; 9359), P53 (Cell Signaling; 9282), STAT-5 (Cell Signaling; 25656), Vinculin (Cell Signaling; 13901).

Digital Droplet PCR

A ddPCR assay to detect the BCL-2 NM_000633.2:c.302G>T, p.(Gly101Val) variant using forward and reverse oligonucleotide primers with locked nucleic acid probes against wild-type and mutant sequence was designed as follows: Forward primer, 5'-CTGGACATCTCGGCGAAG; reverse, ACCTGTGGTCCACCTGA; wildtype probe, HEX-CC+G+G+CGAC+GA-IABkFQ; G101V mutant probe: FAM-CCG+TCG+ACG+ACTTC–IABkFQ (Base with a '+' in front is a LNA base, IABkFQ = Iowa Black® Dark Quencher by IDT). PCR reaction mix contains 1x ddPCR Supermix for Probes (No UTPs), 2 μL of 360 GC enhancer (Applied Biosystems),

primers and probes to a final concentration of 900 nM and 250 nM respectively, and 50 ng of DNA template to a final volume of 25 μL. The reaction is then partitioned into ~20,000 droplets in QX200™ droplet generator. The plate is sealed with Biorad pierceable foil heat seal and sample amplified on C1000 Touch™ Thermal Cycler. Thermal cycling condition: enzyme activation at 95°C for 10 minutes; 40 cycles of denaturation at 94°C for 30 seconds and annealing/extension at 60°C for 1 minute; followed by enzyme deactivation at 98°C for 10 minutes and infinite hold at 4°C. All steps have a ramp rate of 2°C/sec. After PCR, the plate is read on QX200™ Droplet Reader and analyzed in QuantaSoft™ software.

RNA-seq

mRNA was extracted from myeloblasts derived from BM and Spleen of PDXs using RNeasy minikit(Qiagen), following manufacturer's protocol. Stranded RNA-seq libraries were generated using the True-seq RNA exome kit (Illumina) on a Sciclone platform (Perkin Elmer). mRNA underwent fragmentation, cDNA synthesis, and next-generation library synthesis via exome capture and PCR amplification. Libraries were sequenced on a Next-Seq instrument (Illumina) using a paired-end protocol. Paired-end RNASeq samples (75 bp/read) were matched to the human (hg19) and mouse (mm9) genomes and aligned with STAR(Dobin et al., 2013). Each pair of BAM files were then passed onto Xenofilter(Kluin et al., 2018) to eliminate mouse reads; the resulting BAM files were converted back to fastq files. Transcript expression was quantified using Salmon(Patro et al., 2017) and was summarized to gene-level. The count data matrix obtained from Salmon was imported into R using tximport (R package) (Soneson et al., 2015), and then Limma(Ritchie et al., 2015) was applied to perform differential analysis. The output from Limma was then used to perform gene set enrichment analysis (GSEA) using clusterProfiler(Yu et al., 2012).

Rapid Heme Panel Assay

We analyzed the full coding sequences for most genes of a panel of 88 selected based on the presence of recurrent mutations in leukemia (Kluk et al., 2016) in parental and venetoclax resistant PDXs. Briefly, genomic DNA was extracted from banked xenografted tumor cells harvested from spleen (Qiagen DNA mini kit). DNA underwent customized hybrid-capture target enrichment (SureSelect, Agilent) and Illumina NextSeq 550Dx, 150bp paired-end reads sequencing followed by UMI correction (Fgbio V0.4.0). In addition, genomic DNA from the splenocytes of a normal NSG mouse was sequenced in order to enhance species-specific filtering of human reads. Variants were called using Vardict (v1.6.0) and copy number variations (CNV) were called using Robust CNV (developed internally). FLT3-ITD sequencing was carried out using internally developed PCR assay (TsaiITD).

Quantitative PCR for BCL-2 Family Proteins

Molm13 cells plated at $0.5x10^6$/mL and treated with venetoclax, S63845, or DMSO for 1, 2 and 4 hours. Cells were then spun down, media was aspirated, and pellets were stored at -80C. RNA extractions were performed using RNeasy mini kit (Qiagen) per manufacturer's instructions. RNA yield was quantified by nanodrop. RNA was converted into cDNA using the High-Capacity cDNA Reverse Transcription Kit (Applied Biosystems). Quantitative PCR was performed using Taqman Fast Advanced Master Mix (Life Technologies) and Taqman probes indicated in Table S3 (Life Technologies) for *BIM* (Hs00708019_s1), *BAX* (Hs00832876_g1), *BAK* (Hs00832876_g1), *BCL2* (Hs00708019_s1), *BCLXL* (Hs00169141_m1), *MCL1* (Hs00172036_m1), *NOXA* (Hs00560402_m1), *BAD* (Hs00188930_m1), *BID* (Hs00609632_m1), *HRK* (Hs00705213_s1), and *GAPDH* (Hs99999905_m1). PCR cycles were run using the 7500 Real-Time PCR Fast machine with the standard cycle parameters.

QUANTIFICATION AND STATISTICAL ANALYSIS

For clinical response and BH3 profiling correlative studies, comparison of responders and non-responders was determined by one-sided Wilcoxon rank-sum test. Overall survival for the animal study was established by the Kaplan-Meier method using the log-rank test and considered significant at the <0.05 level. Venetoclax and S63845 synergy was calculated using the Loewe method using combenefit program (Di Veroli et al., 2016). Determination of statistical significance was calculated using a Student's t-test or one-way ANOVA using Prism 8 software (GraphPad).